Technical Report No.HWR 88-010 October 1988

EXPERIMENTAL INVESTIGATION OF SEEPAGE THROUGH HETEROGENEOUS POROUS MEDIA

by

James T. Mathieu Jr.
Research Assistant

T.-C. Jim Yeh
Principal Investigator
Assistant Professor

Dept. of Hydrology & Water Resources
The University of Arizona
Tucson, Arizona 85721

Technical Reports on
Natural Resource Systems

Final Report

EXPERIMENTAL INVESTIGATION OF SEEPAGE THROUGH HETEROGENEOUS POROUS MEDIA

Submitted to

The National Science Foundation

By

James T. Mathieu Jr.
Research Assistant

T.-C. Jim Yeh
Principal Investigator
Assistant Professor

Deparment of Hydrology
and Water Resources
University of Arizona
Tucson, AZ 85721

September 1988

Grant: CEE 819214

ACKNOWLEDGEMENT

Financial support for this research was provided by the National Science Foundation (Grant: CEE 819214).

TABLE OF CONTENTS

LIST OF ILLUSTRATIONS

LIST OF ILLUSTRATIONS (continued)

LIST OF ILLUSTRATIONS (continued)

LIST OF TABLES

ABSTRACT

Five sand tank experiments were conducted to investigate the behavior of unsaturated flow in heterogeneous porous media and to test the recent stochastic theories of Yeh et al. (1985a, b, c) and Mantoglou et al. (1987a, b, c) on flow through unsaturated porous media. The hydraulic properties $\theta(\psi)$ and $K(\psi)$ of the medium and coarse sand used in the experiments were measured with various laboratory columns. Fourteen medium and coarse sands were alternately layered in the 2.38 m long x 1.12 m high x 0.1 m thick sand tank. Water was infiltrated from a point source for three of five experiments and from a channel source for two experiments. An array of 62 tensiometers were used to record the capillary tension head distribution during each experiment. The wetting front profiles for the first experiment show the stratified sand effects both the development and dissipation of preferential flow paths. The experimental results qualitatively support stochastic theory of saturation dependent anisotropy. Three of the five experiments agree with the stochastic result of Yeh et al. (1985a and b) that an increase in the variance of the capillary tension head (soil becomes drier) is proportional to an increase in the mean tension head.

CHAPTER 1

INTRODUCTION

Quantitative models of water and contaminant movement in the unsaturated zone are important investigative tools in the fields of hydrology, agriculture and waste management. During the past three decades, human activity above and below the land surface has created a rapid increase of environmental problems in the unsaturated zone. Solutions to these problems require innovative field techniques and quantitative flow models. Scenarios of fluid flow in the unsaturated zone include recharge of potable water for storage in an aquifer, migration of agricultural pesticides to the water table, and leakage of hazardous compounds from subsurface storage tanks. From the viewpoint of the hydrologist, flow of water and dissolved contaminants through the unsaturated zone is the physical process that links the land surface hydrologic flow system with the underlying ground-water flow regime. Freeze and Cherry (1979) estimate nearly 50% of municipal and industrial water consumption in the western United States in 1970 was from ground water. Thus, proper management of ground-water resources hinges on the scientist's and engineer's understanding of unsaturated flow processes and ability to accurately predict flow in the unsaturated zone.

Classical analyses of transport processes in the unsaturated zone utilize the simplifying assumptions that the porous media is homogeneous and isotropic or homogeneous with constant anisotropy (Philip, 1969; and McKee and Bumb, 1988). Analyses of infiltration and redistribution of water in unsaturated soils and sediments have also been simplified by assuming one-dimensional vertical flow. While these simplified analyses contribute to understanding 'ideal' flow systems, they do not incorporate the spatial variability in soil properties and multi-dimensional flow observed in the natural environment. Spatial heterogeneity has been well documented in the past two decades by investigators such as Stockton and Warrick, (1971);

Nielson et al. (1973), Carvallo et al. (1976), and Stephens et al. (1988).

The two fundamental hydraulic soil properties that control flow in the unsaturated zone are the soil-water characteristic curve $\theta(\psi)$ and the unsaturated hydraulic conductivity $K(\psi)$. These functional parameters $\theta(\psi)$ and $K(\psi)$ describe the soil-water content and hydraulic conductivity dependence on the capillary tension head. Figures 1a and 1b show the $\theta(\psi)$ and $K(\psi)$ curves for different spatial locations within two agricultural soils. These figures illustrate the large degree of spatial heterogeneity within a mappable soil unit (Mantoglou and Gelhar, 1987). Stockton and Warrick (1971) show that a 20 to 30 percent variation in predicted unsaturated hydraulic conductivity can result from water contents within one standard deviation of an average water content in a 40 hectare area of a Pima clay loam.

An excellent illustration of spatial variability in sediment profiles is the geologic cross sections of a 30 x 30 meter plot in Socorro, New Mexico (Stephens et al., 1988). The vertical cross sections in Figure 2 show the sediment profile is stratified and individual layers are both continuous and discontinuous. Particle size fractions in the two cross sections vary from clay to cobble and saturated hydraulic conductivity for samples of three bore holes at the Socorro site range over five orders of magnitude.

In light of the spatial variability of soil and sediment properties in the natural environment the question arises:

To what extent does spatial variability effect flow in the unsaturated zone and are the assumptions of homogeneity, isotropy and one-dimensional flow sufficient to accurately predict flow in the unsaturated zone?

The field and laboratory experiments briefly discussed below illustrate the effect of sediment stratification on flow in large and small-scale unsaturated systems.

Mantoglou and Gelhar (1987) report on the observation of Trauntwein et al. (1983) at a waste disposal evaporation pond. The contaminant plume at this site

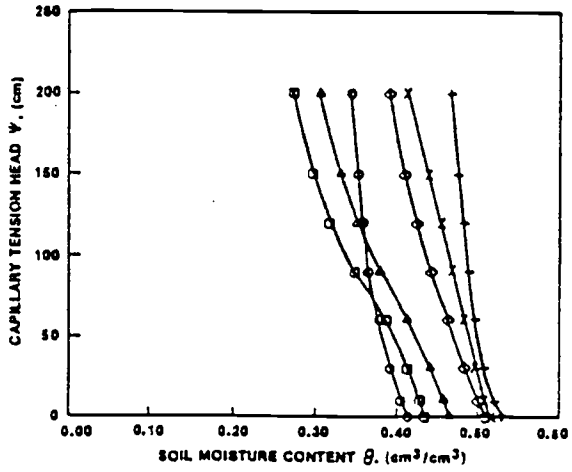

(a)

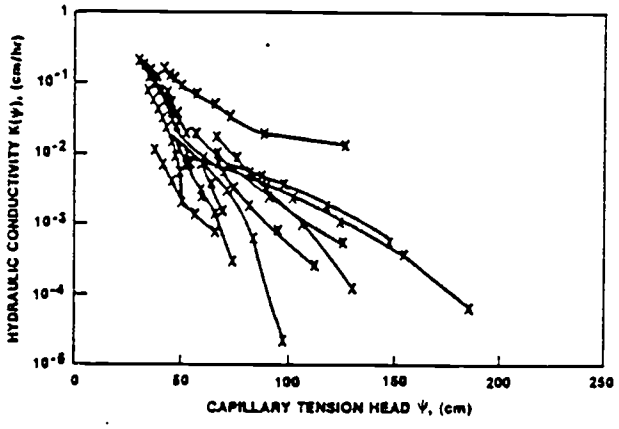

(b)

Figure 1. (a) $\theta(\psi)$ for the Panoche silty clay loam (Nielsen et al., 1973). (b) $K(\psi)$ for the Maddock silty clay loam (Carvallo et al., 1976). Each curve in (a) and (b) corresponds to a different spatial location.

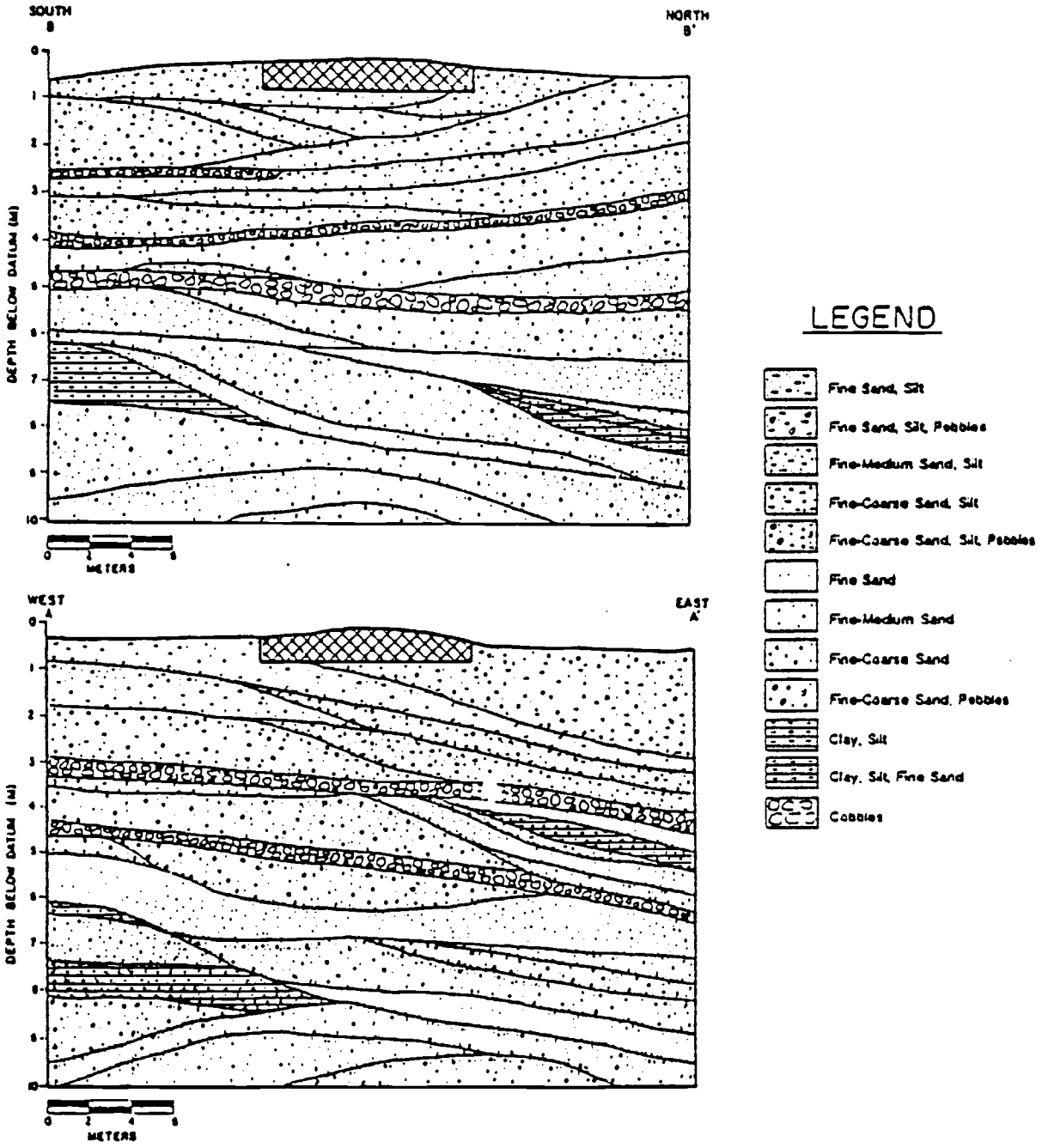

Figure 2. Geologic cross sections at the Socorro site. Vertical exaggeration: 2x. Hatched area shows drip irrigation system (Stephens et al., 1988).

extended 2.000 meters laterally in the stratified sediments beneath and surrounding the pond. Mantoglou and Gelhar (1987) suggest that movement of the waste water may be due to both the formation of perched saturated zones and large lateral unsaturated conductivity, i.e. large relative to the vertical conductivity.

Stephens et al. (1988) infer the sediment stratification at the Socorro site (see Figure 3) facilitated the lateral spreading of an infiltrating water plume. Specifically, they report the wetting front advanced seven meters vertically and two to three meters laterally from the edge of the irrigation (source) plot after 80 days of irrigation. Futhermore, the vertical rate of advance of the wetting front, measured in two neutron probe holes, decreased as the front moved from texturally finer to coarser layers. This decrease in vertical advance of the wetting front may correspond to an increase in lateral advance of the front.

Palmquist and Johnson (1962) describe an infiltration experiment in an acrylic tank containing three layers of 0.036 mm diameter glass beads interbedded with two layers of 0.47 mm diameter glass beads. The five layers were air dry prior to infiltration. Water was infiltrated from a line source into the top 'fine' layer at rate approximately 13 times the saturated hydraulic conductivity of the fine beads. Palmquist and Johnson (1962) report that the vertical advance of the wetting front stopped at the 'fine' over 'coarse' interface and subsequently the front moved horizontally in the 'fine' layer. This same phenomena is explicitly demonstrated in the film "Water Movement in Soil" by W. H. Gardner (date unknown) in which the vertical advance of the wetting front is impeded at a coarse sand lens. Gardner (date unknown) explains the wetting front enters the sand lens when the water pressure becomes large enough to fill the relatively large pores.

An example of natural heterogeneity effecting the migration of leachate from an oil-gas brine pond is reported by Murphy et al. (1988). Field observations at the site in North Dakota indicate the horizontal component of leachate migration was seven times the vertical component. The extensive leachate migration caused soil

sterility, decreasing crop yields and death of trees in a 200,000 square foot area surrounding the brine ponds.

The behavior of the flow systems discussed above shows that stratification can retard the vertical advance of water and dissolved contaminants while enhancing lateral movement. These studies also suggest the assumptions of homogeneity, isotropy, and one-dimensional flow are not valid if one wishes to predict flow and transport in unsaturated soils and sediments. A recent stochastic analysis by Yeh et al. (1985a, b, and c) incorporates local scale spatial variability of one- and three-dimensional flow systems into macroscopic effective parameters. One such parameter derived by Yeh et al. (1985a, b, c), under steady flow conditions, is the macroscopic saturation-dependent anisotropy relating a soil's anisotropic behavior to measurable physical and hydraulic properties (anisotropy is the ratio of lateral to vertical effective conductivity). The properties included in the saturation dependent anisotropy are the mean and variance of the pore size distribution, the variance of log-saturated conductivity, the vertical correlation scale, layer orientation, and the 'mean' capillary tension head (or water content). In general, the anisotropy parameter increases as the capillary tension head increases, i.e. as the soil-water content decreases. Mantoglou and Gelhar (1987a, b, c) extend the stochastic analysis of Yeh et al. (1985a, b, c) to transient flow conditions. They also conclude the degree of anisotropy depends on the mean capillary tension head and, in addition, the lateral and vertical effective conductivities show significant hysteresis.

The stochastic result of saturation dependent anisotropy is quite attractive for use in solving large scale unsaturated flow problems. However, this parameter and the other stochastic results of Yeh et al. (1985a, b, c) and Mantoglou et al. (1987a, b, c) must be tested against experiments for range of application and physical correctness. Stephens and Heerman (1988) discuss the results of a sand tank experiment which is perhaps the first attempt to validate the saturation dependent anisotropy. The sand tank used in this experiment represents a 150 cm high x 175

cm long, 30 degree wedge from a vertical cylinder. A relatively fine and coarse sand was alternately layered to form 40 layers, each two centimeters thick. Water was infiltrated from a source pipe in the upper two centimeters at the apex of the tank. The hydraulic head distribution was mapped with an array of tensiometers and pathlines were traced with dye. Stephens and Heerman (1988) show that an increase in the angle between specific discharge and hydraulic head gradient vectors is proportional to an increase in anisotropy. Their experimental results show the angle between the two vectors increased from approximately 5 to 70 degrees along one pathline originating at the source. Stephens and Heerman (1988) conclude this result qualitatively supports the saturation dependent anisotropy concept. Other field and laboratory experiments are required to test the stochastic results of Yeh and Gelhar (1985a and b) and Mantoglou and Gelhar (1987a and b).

The primary objectives of this study are: 1) to investigate the behavior of unsaturated flow through heterogeneous porous media and 2) to validate the stochastic results of Yeh et al. (1985a and b) and Mantoglou et al. (1987a and b). The objectives of this study were carried out by conducting five infiltration experiments in a large sand tank which contained stratified sand. The results of the sand tank experiments are presented in this report in the context of the two objectives. The organization of this report is as follows: a) Chapter 2: Design of the Laboratory Experiments and Characterizing the Material Properties, b) Chapter 3: Discussion of Experimental Conditions and Results, and c) Chapter 4: Conclusion.

CHAPTER 2

DESIGN OF THE LABORATORY EXPERIMENTS AND CHARACTERIZING THE MATERIAL PROPERTIES

Each of the five sand-box experiments were conducted in a large polycarbonate tank that contained alternating layers of two distinct quartz sands. The experiments were conducted under different boundary and initial conditions and the energy status of the soil water was monitored with a network of 62 tensiometers. ('Sand' and 'soil' are used interchangeably throughout this text). Unsaturated flow conditions were maintained throughout the flow domain for each experiment with the exception of the source region and lower boundary condition.

This section gives a detailed description of the tank design, the geometric and hydraulic properties of the two sands, the sand packing, the tensiometers, and the design of the source and lower boundary condition. This description is divided into the following 9 topics: 1) sand-box design, 2) sand characteristics, 3) water content-tension characteristics, 4) hydraulic conductivity, 5) sand layering in the sand box, 6) tensiometer design and location in the sand tank 8) fluid source plumbing, and 9) lower boundary condition.

2.1 Sand Tank Design.

The sand tank was constructed from two 2.44 m x 1.22 m sheets and one 2.44 m x 0.61 m sheet of transparent 1.27 cm thick polycarbonate. The sheets were cut with a table saw and joined with solvent cement (methylene chloride) to form the rectangular box (open on top) with the interior dimensions of 2.38 m x 1.12 m x 0.1 m (Figure 3). A support frame of 2.54 cm angle steel was built around the tank to strengthen the cemented joints. This steel was also used to brace against four polycarbonate shelves to prevent the polycarbonate sheets from flexing.

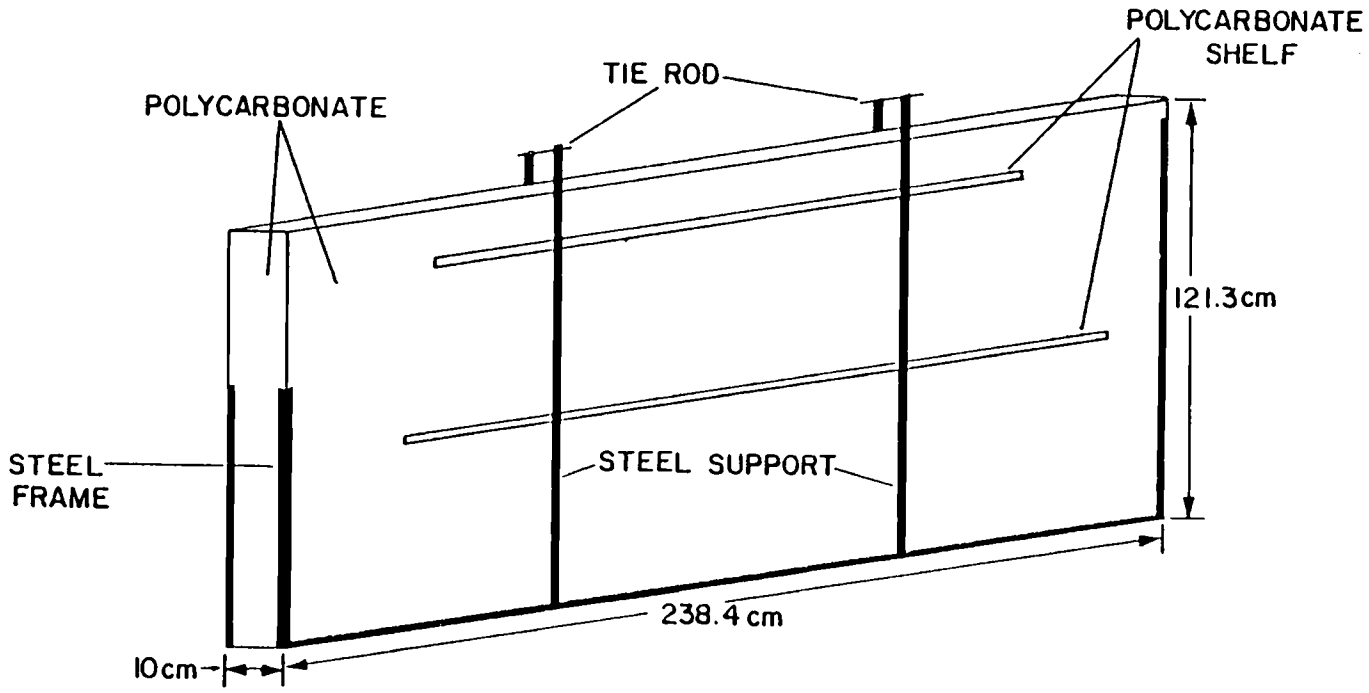

Figure 3. Sand tank and steel frame.

2.2 Sand Characteristics.

Three criteria were used in selection of the medium and coarse sands used in the sand box. First, each sand should be relatively uniform in grain size to minimize heterogeneity on the scale smaller than the thickness of one sand layer. Second, the two sands should have distinct hydraulic properties, but should not differ substantially in grain size. Grain size similarity ensures a sharp interface between the two sands. Third, the two sands should be inexpensive and easily obtained.

2.3 Sand Sieving and Grain Size Analysis.

Four hundred fifty-four kilograms each of a No. 30 and No. 20 quartz sand were purchased from a commercial sand and gravel yard. This sand is typically used for blasting exterior walls of buildings. Even though this sand was commercially sieved, each bag contained size fractions larger and smaller than the range desired for the experiments. As a consequence the No. 30 sand was hand sieved so that it passed through a 0.53 mm (opening dimension) screen and was retained on a 0.23 mm screen. The No. 20 sand was hand sieved so that it was retained on the 0.53 mm screen. Figure 4 shows the cumulative grain-size distribution for the sieved sands. The sieved No. 30 and No. 20 sands plot as medium and coarse sands, respectively, with respect to the U.S.D.A. classification. The terms 'medium' and 'coarse' sand are used in the remainder of this text. Table 1 lists the d_{10} and d_{50} values for the medium and coarse sands.

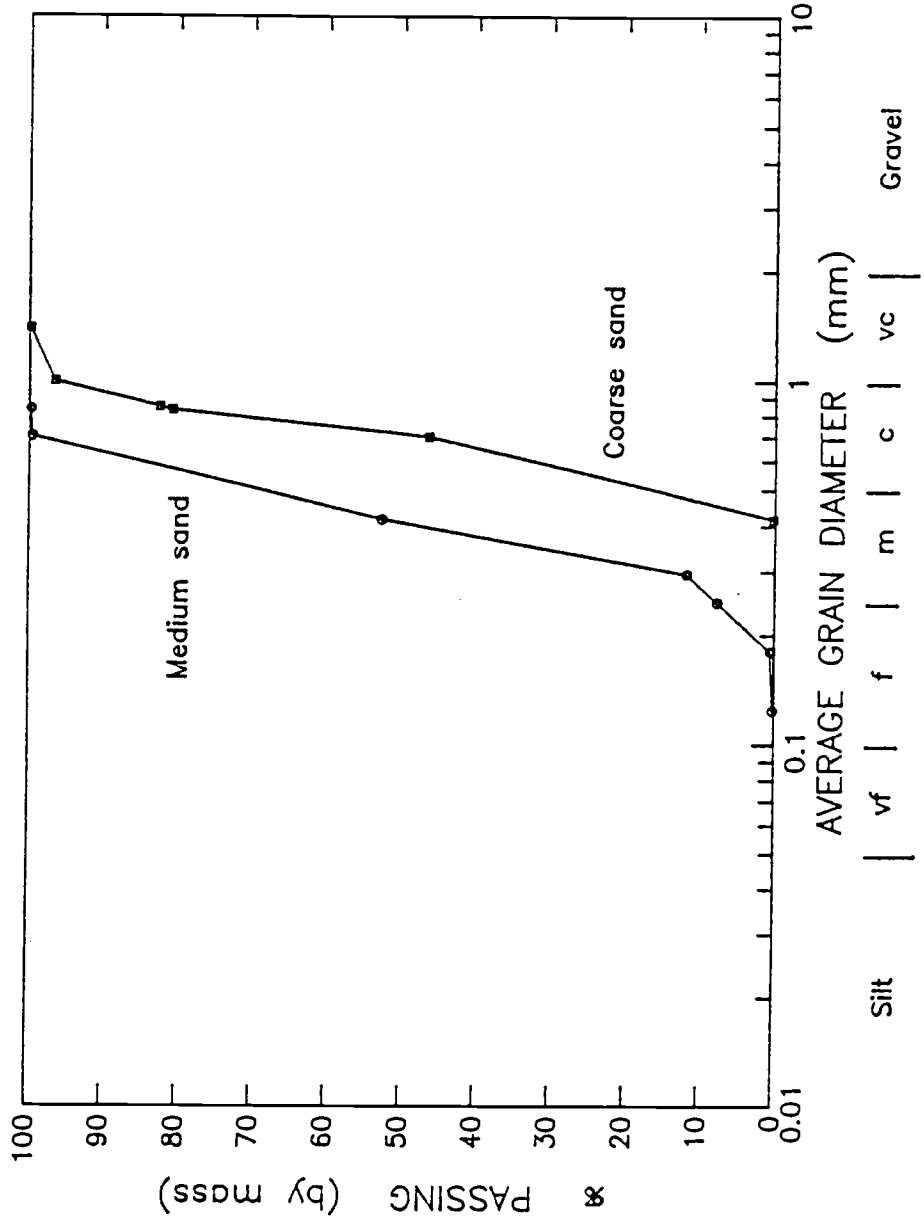

Figure 4. Cumulative grain-size distribution in relation to U.S.D.A. classification.

Table 1: d_{10} and d_{50} values for the medium and coarse sand.

	d_{10} (mm)	d_{50} (mm)
medium sand	0.12	0.30
coarse sand	0.35	0.72

2.4 Bulk Density and Porosity.

The dry bulk density for the medium and coarse sands were determined from ten and eight samples, respectively. The samples were oven dried and repacked from several soil-hydraulic tests. Table 2 lists the dry bulk density and porosity with the arithmetic mean and sample standard deviation. The porosity, n_p, was computed from the relation:

$$n_p = 1 - \frac{\rho_b}{\rho_s} \tag{1}$$

where ρ_b is the dry bulk density (g/cm^3) and ρ_s is the particle density (assumed 2.65 g/cm^3). The mean porosities are 0.449 for the medium sand and 0.435 for the coarse sand.

Table 2: Dry bulk density and porosity for the medium and coarse sand.

	Medium sand		Coarse sand	
	ρ_b	n_p	ρ_b	n_p
	1.49	0.438	1.55	0.414
	1.53	0.423	1.50	0.434
	1.5	0.435	1.48	0.442
	1.5	0.435	1.50	0.434
	1.48	0.44	1.53	0.442
	1.44	0.456	1.46	0.448
	1.42	0.464	1.49	0.439
	1.43	0.462	1.45	0.451
	1.4	0.47	1.41	0.467
Mean	1.46	0.449	1.5	0.435
S.D.	0.042	0.016	0.032	0.012

2.5 Water Content - Tension Head Characteristics.

Water content - capillary tension head data for the medium and coarse sands were obtained by using the apparatus and method described by Baker et al. (1974). This method involves placing a soil sample (75 to 100 cm^3 in this study) on a saturated porous plate that is hydraulically connected to a column of water. The sample is first saturated and then the column is incrementally lowered to obtain drying $\theta(\psi)$ data and raised to obtain a wetting $\theta(\psi)$ data. Three replicate samples each of the medium and coarse sand were tested in this apparatus. These data are plotted in Figure 5 together with the fitted functional relation:

$$\theta = \theta_r + \frac{\theta_s - \theta_r}{\left[1 + (\alpha\psi)^n\right]^m} \qquad (2)$$

where θ is the volumetric water content (cm^3/cm^3), ψ is the capillary tension head (cm H_2O), θ_s is the saturated water content, θ_r is the residual water content, α, n, and m are fitting parameters in which $m = 1 - 1/n$. The function (2) fits both the medium and coarse sands quite well except for tension ranges of 35-120 cm and 20-80 cm, respectively (Figure 5).

The non-linear least squares program SOHYP (Van Genuchten, 1978) was used to determine the parameters α, n, and m by fitting (2) to the data points in Figure 5. The parameters α, n, and m can then be used to express the functional form of the relative hydraulic conductivity $K^r(\psi)$. The program gives the user the option to use the relative hydraulic conductivity models of Burdine (1953) or Mualem (1976).

The specific water capacity, $C(\psi)$, as a function of capillary tension head for the medium and coarse sands is plotted in Figure 6. $C(\psi)$ is a functional parameter that characterizes a soil's volumetric ability to store water at particular tension head

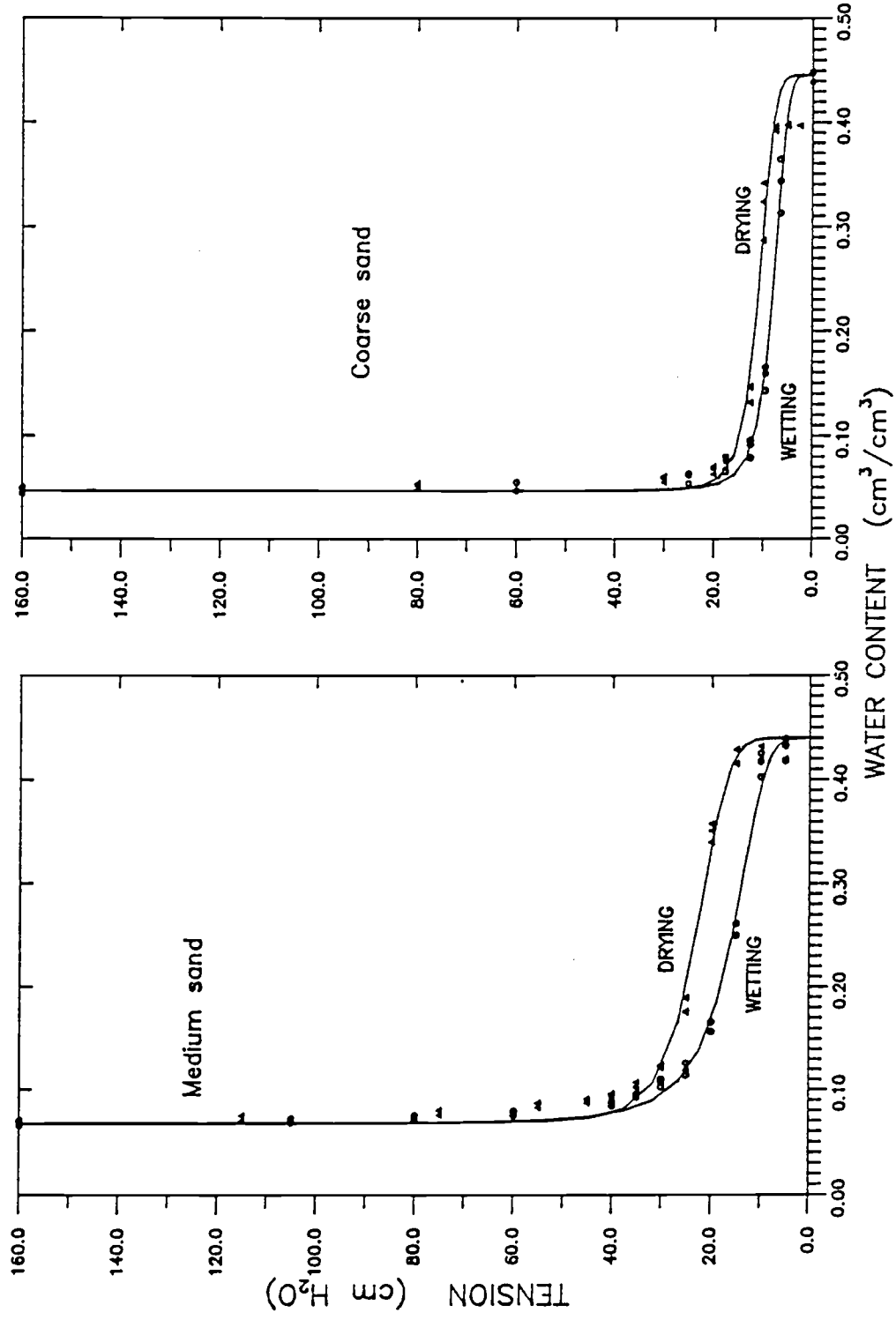

Figure 5. Water content - tension head characteristics for the medium and coarse sand.

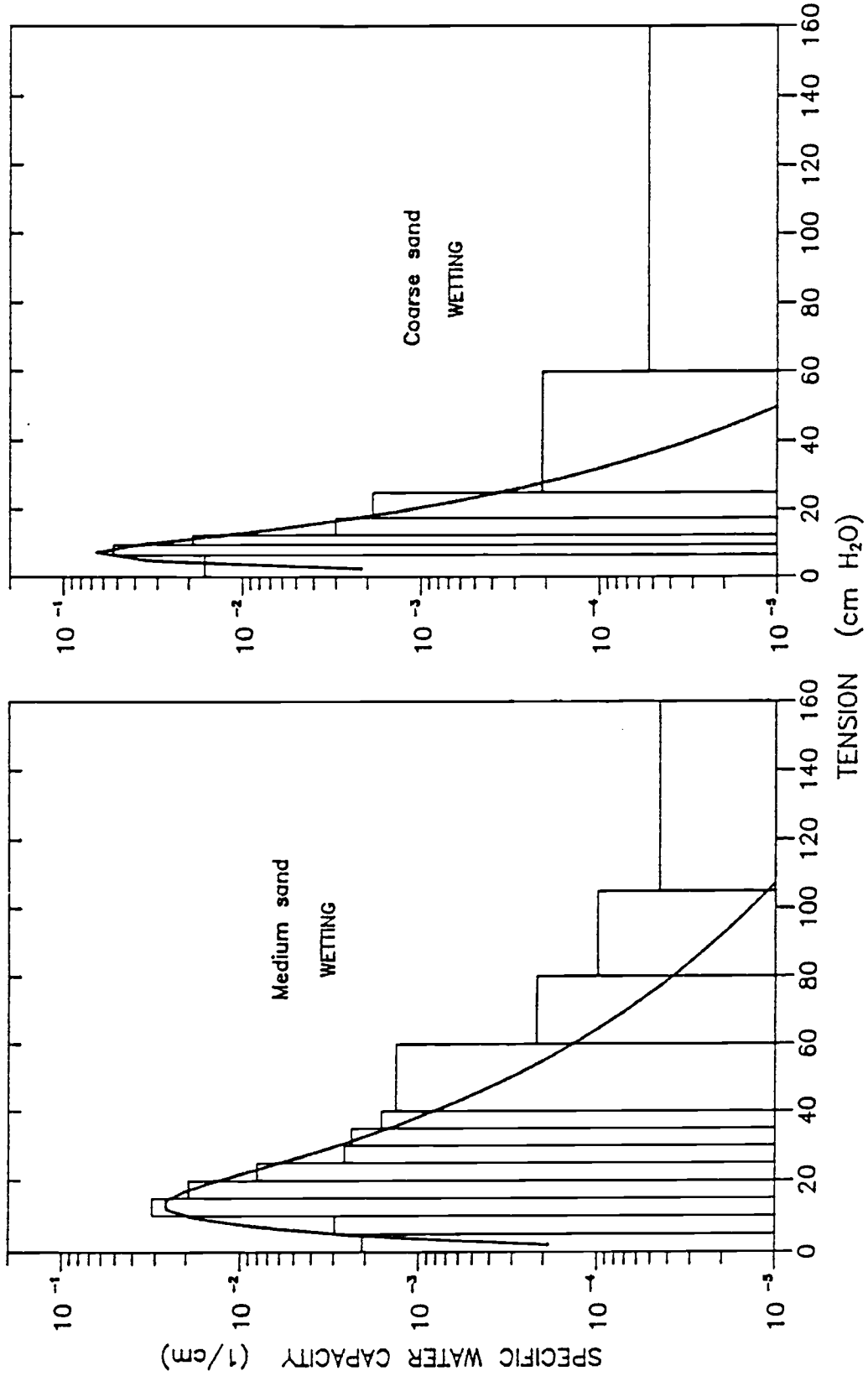

Figure 6. Specific water capacity - tension head characteristics for the medium and coarse sand.

values. In terms of the physical interaction of water and porous media, pore geometry and pore size distribution control the functional form $C(\psi)$. The histograms in Figures 6a and 6b represent the discrete capacity distribution, $C(\psi_{[i,i+1]})$, computed from:

$$C(\psi_{[i,i+1]}) = \frac{\theta_{i+1} - \theta_i}{\psi_{i+1} - \psi_i} \tag{3}$$

where θ_i is the water content measured at each tension, ψ_i. The two capacity distributions are for the wetting-cycle data from the water content - tension data in Figure 5. The continuous water capacity curves in Figures 6a and 6b are computed from the derivative of (2) with respect to ψ which can be expressed as:

$$C(\psi) = \alpha\ n\ m\ (\theta_r - \theta_s)\ \frac{(\alpha\psi)^{n-1}}{\left[1 + (\alpha\psi)^n\right]^{m+1}} \tag{4}$$

where the variables are defined above. Table 3 summarizes some physical and statistical parameters of the $\theta(\psi)$ and $C(\psi)$ relationships for the medium and coarse sands.

Table 3: Hydraulic and statistical parameters for the medium and coarse sand.

	Medium sand	Coarse sand
Average θ_r	0.067 (.015)[0]	0.047 (.012)
Average θ_s	0.44 (extrapolated)	0.446 (.005)
α[1]	0.0693 w 0.0449 d	0.1343 w 0.0956 d
n[1]	4.53 w 7.28 d	5.28 w 6.81 d

[0]Numbers in parentheses are sample standard deviations of three samples.
[1]Statistical parameters from Mualem 2, Van Genuchten (1978).
w = parameter estimated from wetting data
d = parameter estimated from drying data

2.6 Hydraulic Conductivity.

Saturated hydraulic conductivity, K_{sat}, for the medium and coarse sands was measured with a steady state column experiment similar to the apparatus shown in Freeze and Cherry, (1979). The sand column length was approximately 15 cm and the diameter was 4.52 cm. The column was repacked five times for the medium sand and six times for the coarse sand. Table 4 summarizes the saturated hydraulic conductivity statistics.

Table 4: Saturated hydraulic conductivity for the medium and coarse sand.

	Mean K_{sat} (cm/s)	S.D.	Repacked samples
Medium sand	0.078	0.005	5
Coarse sand	0.136	0.013	6

Unsaturated hydraulic conductivity as a function capillary tension head, $K(\psi)$, was determined by using the unit gradient approach in an acrylic tube. Harvey (thesis, 1989 expected) assembled the column and conducted a drying experiment for the coarse sand. The column in this experiment was 57.5 cm long and 5.1 cm in diameter. Tension head in the column was measured with four tensiometer-manometers that were spaced 7 cm apart and located in the upper one half of the column. A set of drainage-equilibration tests were conducted in which the tension head measured at the four tensiometers equilibrated to the same soil-water tension value for a given steady flux rate. The unsaturated conductivity curve was determined for equilibrated tension values by:

$$K(\psi_*) = \frac{q}{I}, \quad \text{at each } \psi_* \tag{5}$$

where q is the steady flux rate measured at the inflow and outflow ports of the column and I is the hydraulic gradient (I = 1 in this experiment).

The $K(\psi)$ data is plotted in Figure 5. The dashed curves in Figure 7 represent the $K(\psi)$ relationship derived by fitting (2) to the $\theta(\psi)$ data for the drying cycle of the coarse sand. The fitting parameters α, n, and m together with two measured K_{sat} values, 0.08 and 0.136 cm/s, are used in the form:

$$K(\psi) = K_{sat}K^{r(\psi)} = K_{sat}\frac{\left\{1 - (\alpha\psi)^{n-1}\left[1 + (\alpha\psi)^{n}\right]^{-m}\right\}^{2}}{\left[1 + (\alpha\psi)\right]^{.5m}} \tag{6}$$

This two parameter functional form of $K(\psi)$ is derived by Mualem (1976) and used in the program SOHYP, by Van Genuchten (1978).

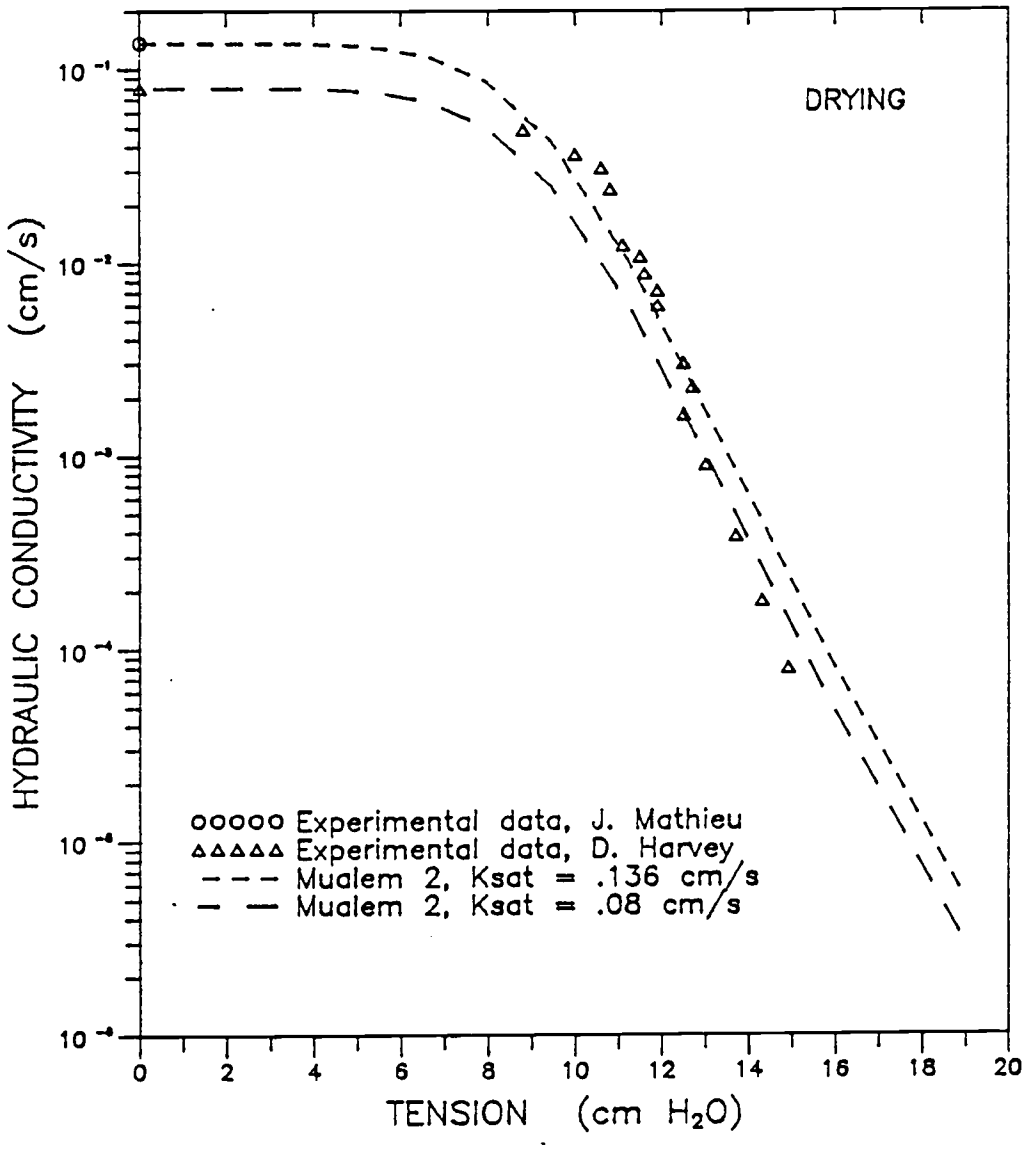

Figure 7. Experimental data (triangles) and predicted curves (dashed) for unsaturated hydraulic conductivity of the coarse sand: Drying Cycle.

The predicted $K(\psi)$ relation obtained from SOHYP for the wetting cycle of the medium and coarse sands is plotted in Figure 8. Again, these curves were derived by using the fitting parameters α, n, and m with the corresponding K_{sat} value. Data is currently being collected for the $K(\psi)$ relationship for wetting cycles of the medium and coarse sands and this data will be compared to the predicted curves in Figure 8.

2.7 Sand Layering in the Sand Box.

The medium and coarse sand interface positions are shown in Figure 9. The individual layers were introduced into the sand box by hand pouring the sand through a stack of three, 3.17 mm (opening size) screens that were constructed to cover the top of the polycarbonate tank. The 3.17 mm screens were approximately 9 cm apart and were used in the sand layering process to facilitate a homogeneous grain distribution within each medium or coarse sand layer (Heerman, 1986). The top of each layer was lightly tamped at the desired interface position with a 72 cm x 9.9 cm board before introducing the overlying sand layer.

The criteria used to determine the layer thickness and the number of layers was that each layer should be thick enough to contain its distinct hydraulic characteristics and small enough to ensure the overall domain is multi-layered. The bottom coarse sand layer thickness was set at 18 centimeters and all overlying layers at eight centimeters. The orientation of each layer was to be horizontal. Figure 10 shows that neither the layer thickness nor layer orientation is eight centimeters and horizontal. The top six interface positions are plotted in this figure with a 2.15x vertical exaggeration. The polycarbonate sheets bowed out as the top two layers were poured into the box. This produced the layer thinning and slumping in the center one third of the domain (Figures 9 and 10). The upper polycarbonate shelf was cemented to the sand box after the polycarbonate sheets had bowed out to prevent further strain of the polycarbonate (Figure 3).

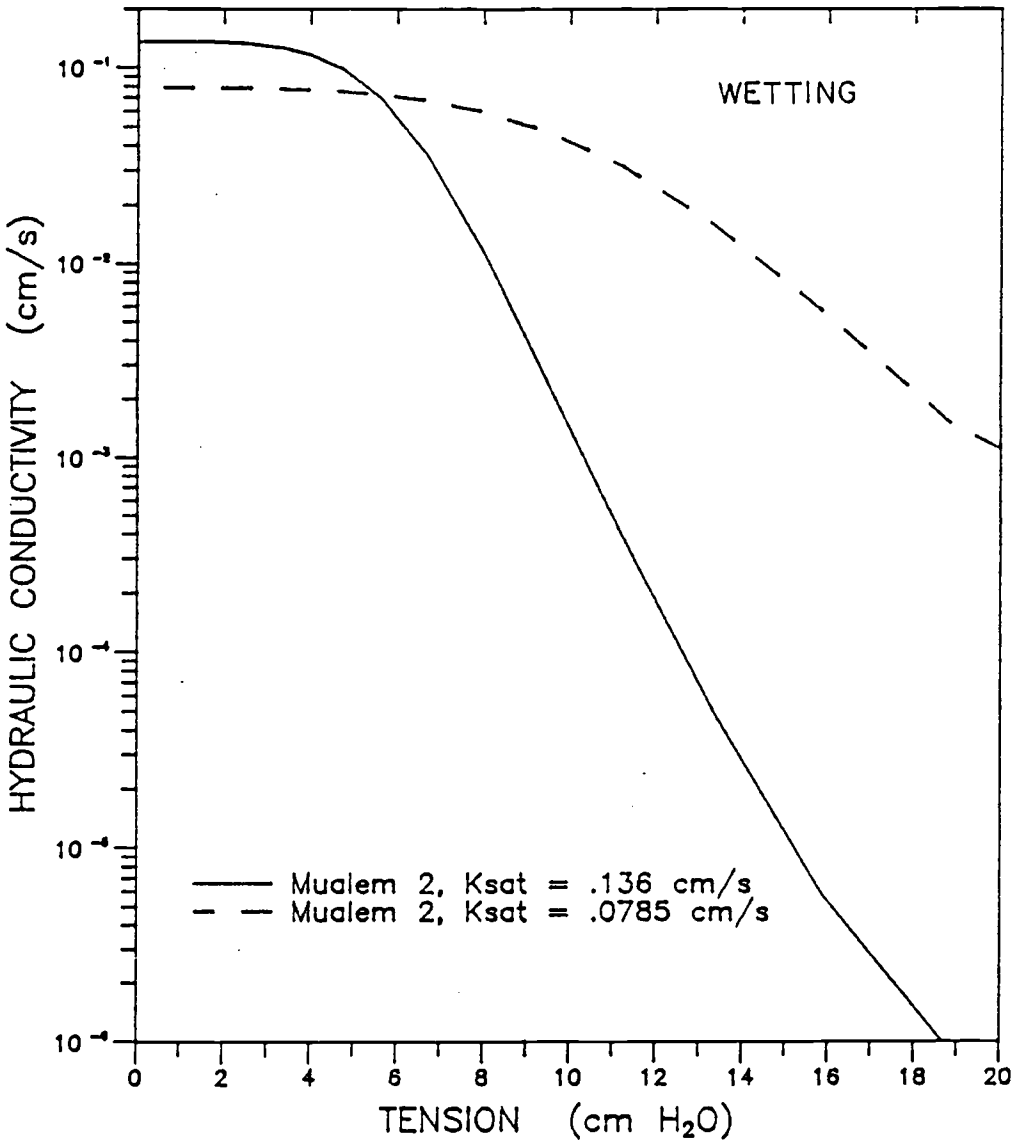

Figure 8. Predicted unsaturated hydraulic conductivity for the medium (dashed) and coarse (solid) sand: Wetting Cycle.

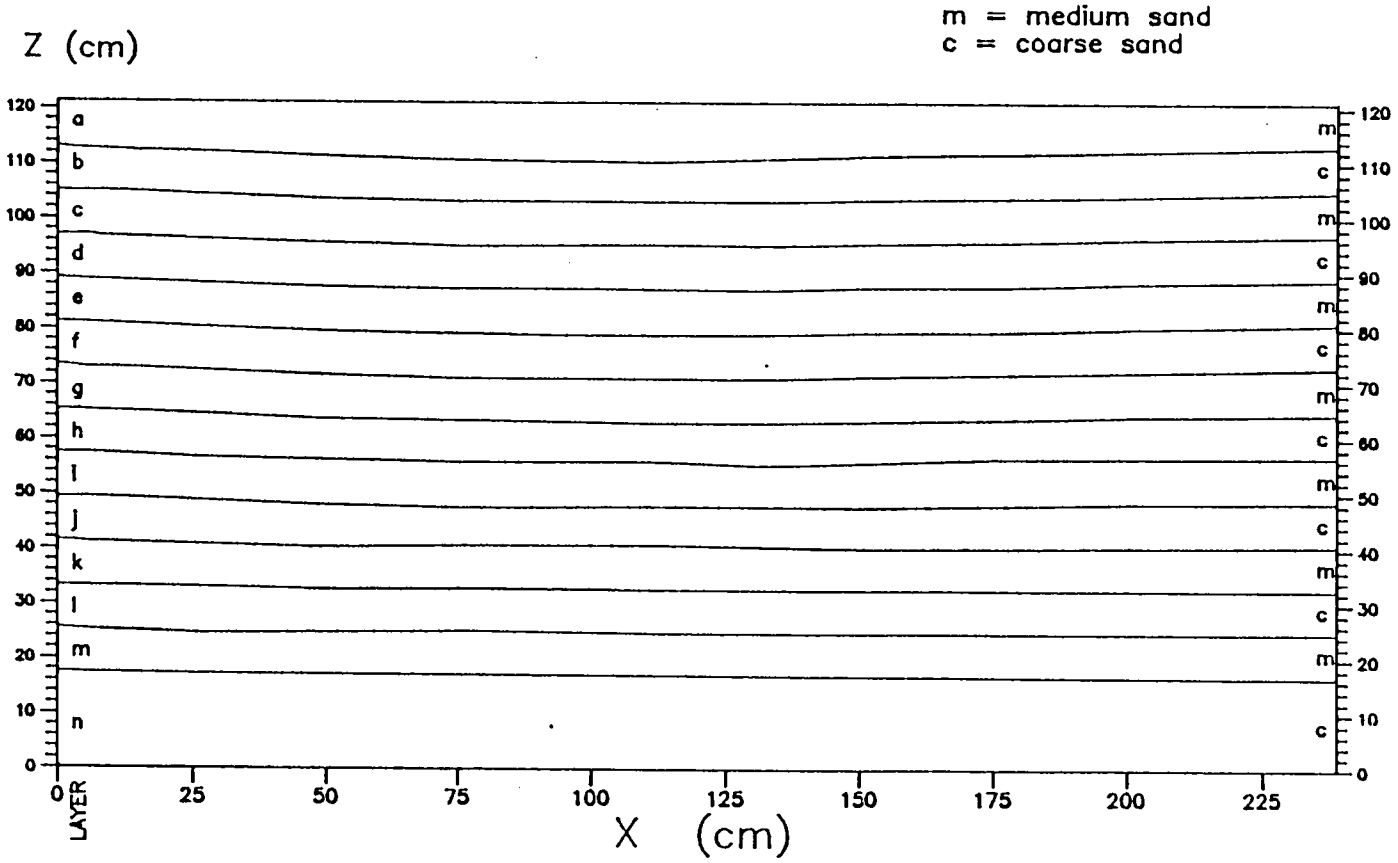

Figure 9. Medium - coarse sand interface positions in the sand box. Layers are labeled 'A' through 'N' from top to bottom.

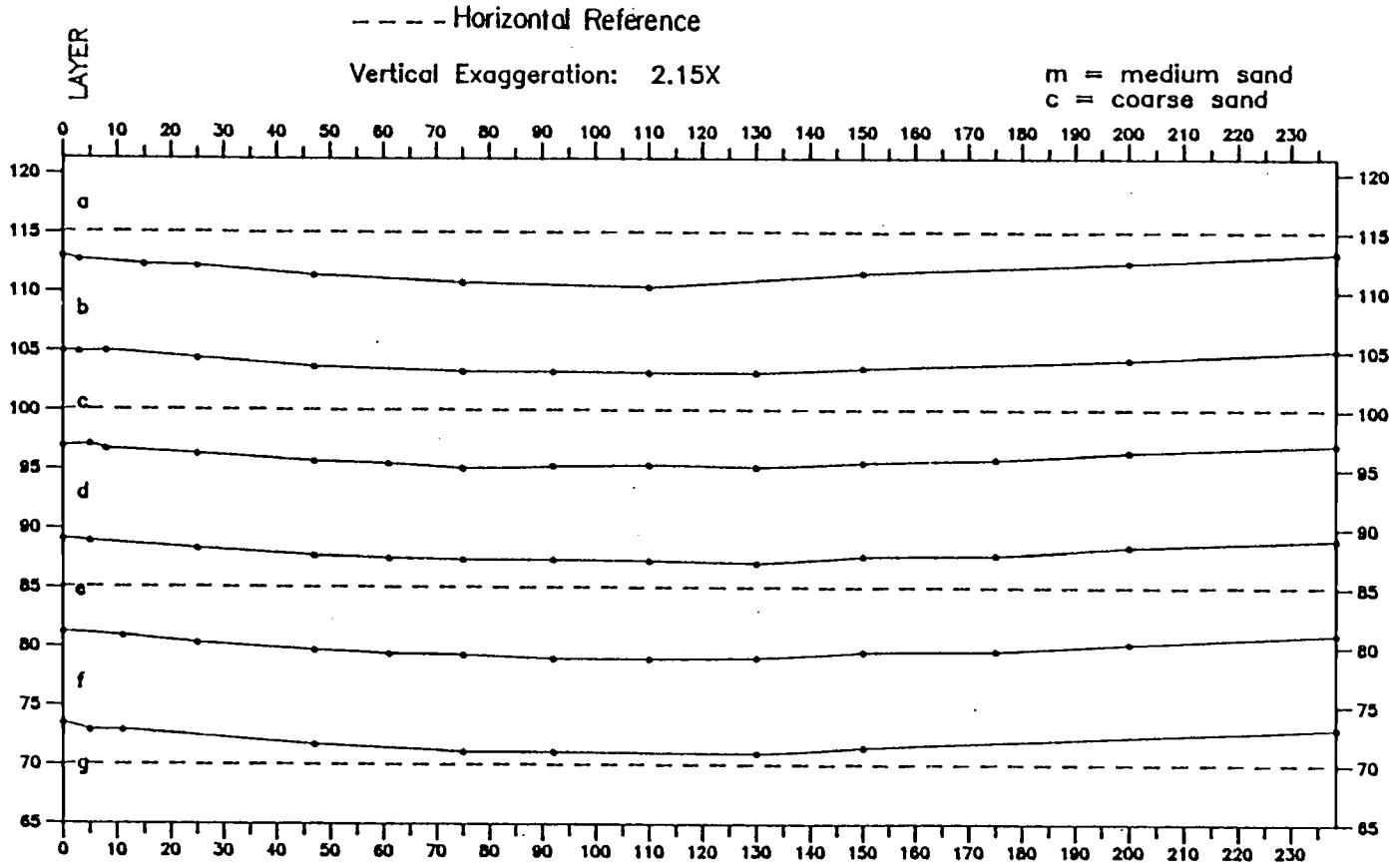

Figure 10. Upper six interface positions in the sand box. The interfaces are not horizontal. Vertical exaggeration: 2.15x.

2.8 Tensiometer Design and Location in the Sand Tank.

Sixty water manometer-tensiometers were used to measure the fluid potential (capillary tension head) during each of the sand-box experiments (Figure 11). The design of the tensiometers and their position in each sand layer relative to the two polycarbonate walls is shown in Figure 12. Manometer tubes for 60 tensiometers were hung on pegboard panels. A millimeter scale was attached to each pegboard so that water levels in the manometer could be rapidly read and recorded. The accuracy of this tensiometer-manometer instrument at an equilibrium condition is estimated to be ±0.05 cm H_2O.

Fluid potential in two tensiometers used in the experiments was measured with a Tensimeter. The Tensimeter is a three component instrument shown in Figure 13. This unit is distributed by Soil Measurement Systems, Las Cruces, N.M. The tensiometer-Tensimeter system for measuring fluid potential was determined to be inferior to the tensiometer-manometer for measuring equilibrium potential in the medium and coarse sands. The reason for this is that small motion of the syringe in the septum stopper would produce changes on the digital display of one and two centimeters of H_2O. Compare this to the estimated ±0.05 cm H_2O accuracy of the tensiometer-manometer. Based on the wetting curve for the coarse sand, 8 cm H_2O ±1 cm H_2O would result in water content estimates of 0.304 (7 cm H_2O) to 0.184 cm^3/cm^3 (9 cm H_2O). This indicates that for the well-sorted medium and coarse sands, water content estimates within certain potential ranges are highly sensitive to instrument accuracy.

The location of all 62 tensiometers in relation to the medium and coarse sand interfaces is shown in Figure 14. The tensiometer ports were drilled before the sand was packed in the tank and each port was plugged with a rubber stopper during the sand packing procedure. Two additional holes were drilled on each edge of the sand box and covered from the inside with screen. These two ports were designed as exit points for the release of air pressure during an infiltration

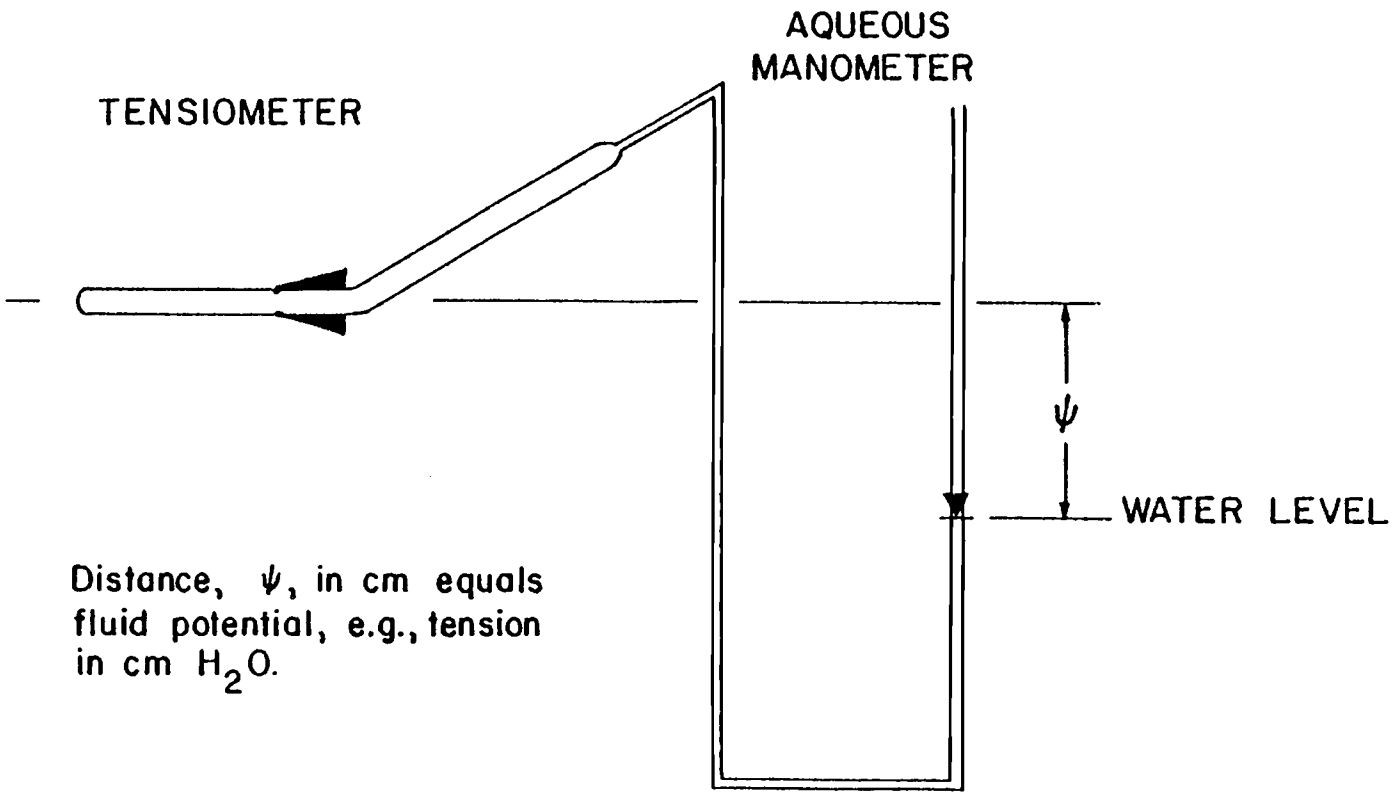

Figure 11. Method of measuring the capillary tension head in wet sand.

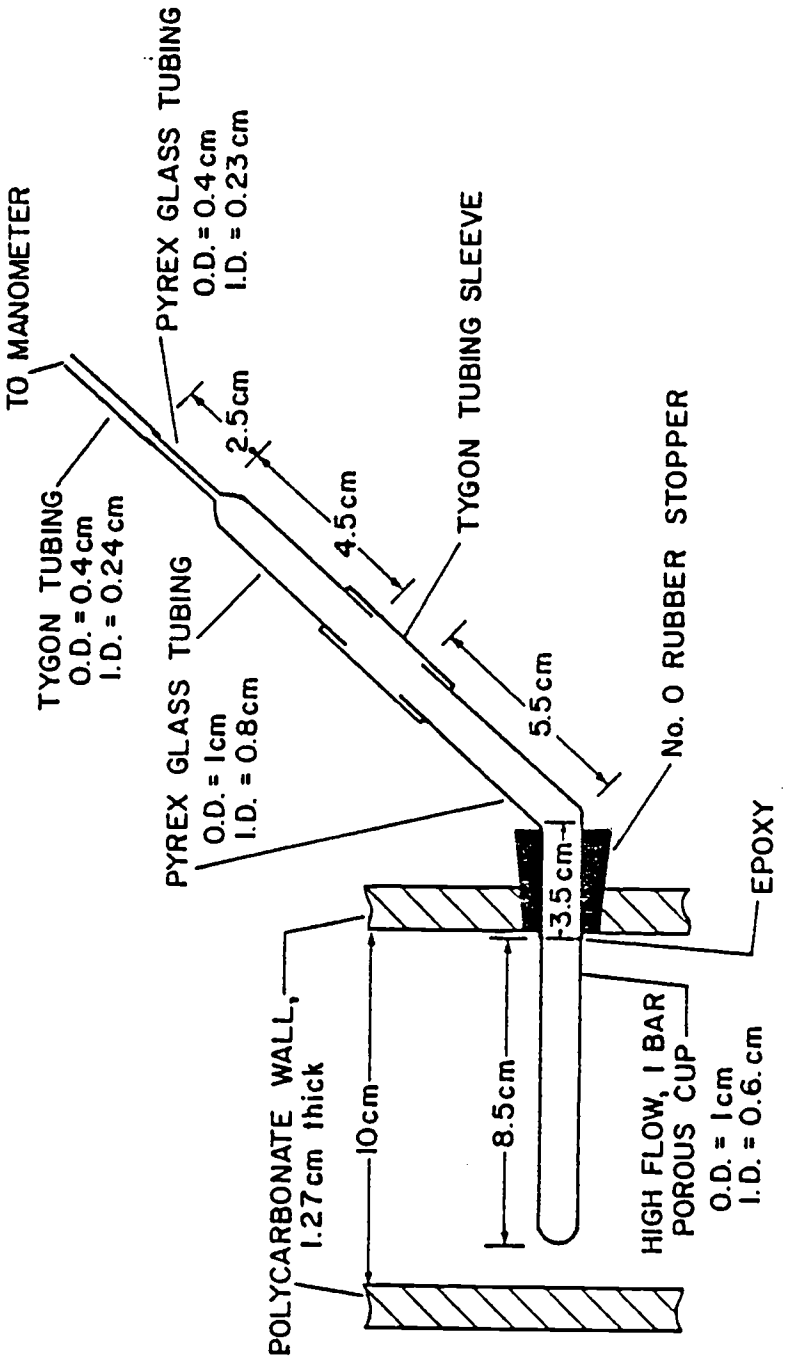

Figure 12. Tensiometer - manometer design and position relative to the sand tank walls.

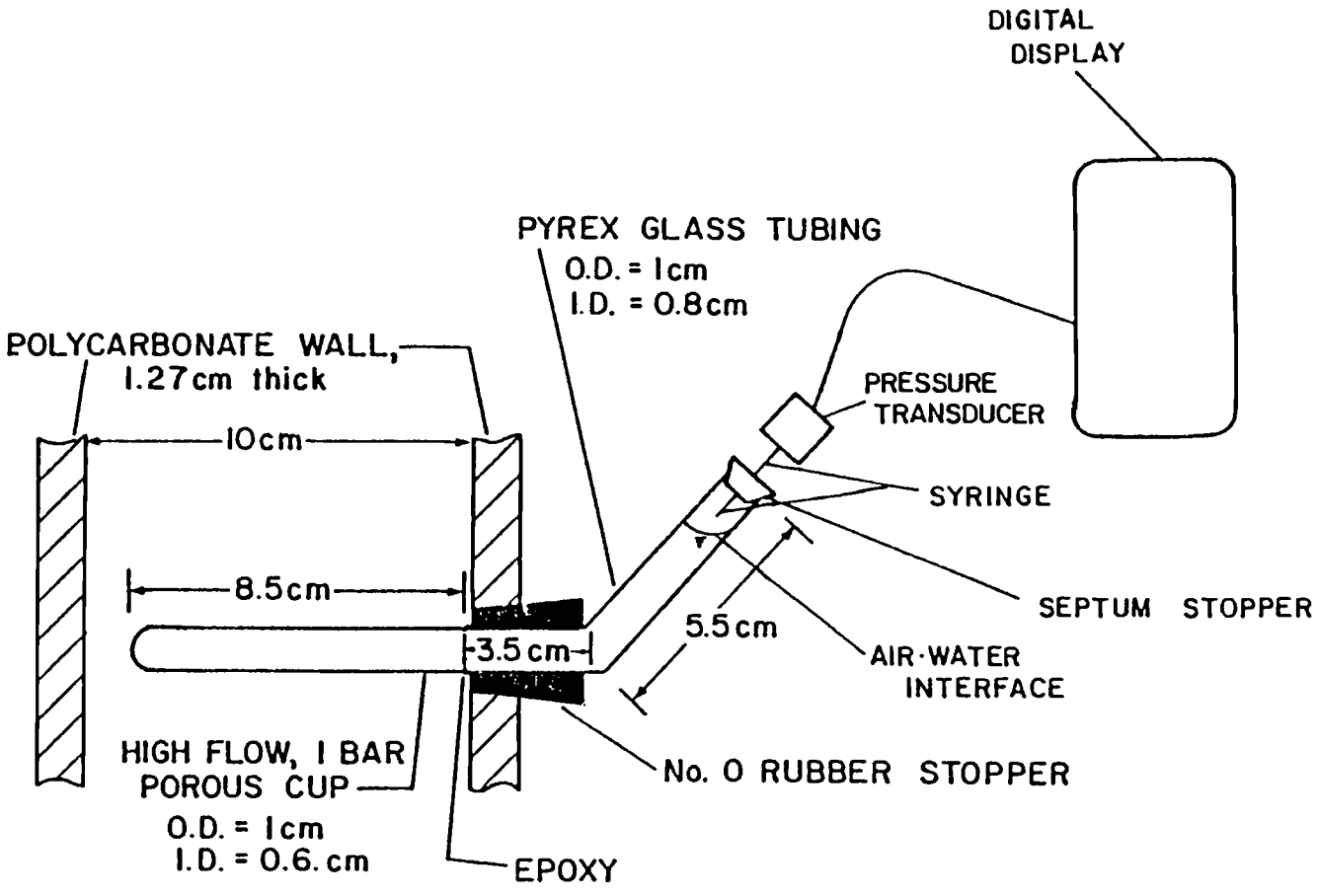

Figure 13. Tensiometer - Tensimeter method for measuring capillary tension head.

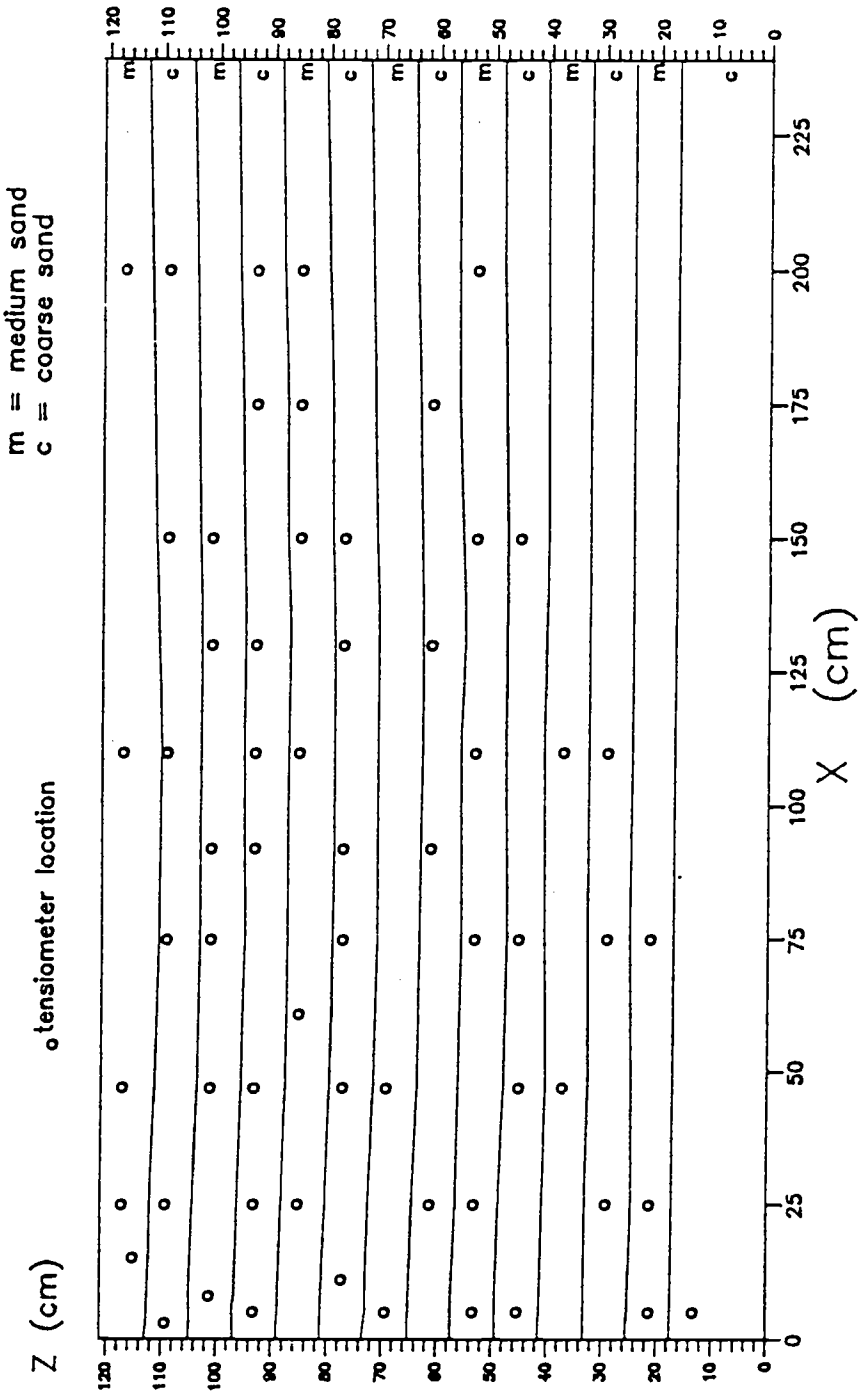

Figure 14. Tensiometer port locations relative to interface positions.

experiment. The choice of tensiometer location was based on the criteria that 'average' pressure gradients would be greater near the fluid source, and therefore sampling density should be higher near the source. Each tensiometer port was also positioned so that the tensiometer would sample the capillary tension head in the center of each layer. However, this criteria was not met since the layers slumped and thinned during the sand packing procedure.

2.9 Fluid Source Geometry and Design.

Water was infiltrated for Experiments 1-5 at prescribed rates in the upper left corner of the flow domain. Figure 15 shows a schematic diagram of the source tube (a point source in 2-D) used in Experiments 1-3 and the source box (a channel source in 2-D) used in Experiments 4 and 5. A fine sponge was placed in the source tube shown in Figure 15a to evenly distribute water out of ten 1.5 mm diameter holes. For experiments 1, 2, and 3 the tube was placed directly on the top surface (the medium sand). A 10 cm x 10 cm piece of cheese cloth between two pieces of 0.11 mm polyethylene mesh was placed between the sand channel surface and the source box used in Experiments 4 and 5 (Figure 15b). Water flowed from the source box via 190 1.5 mm diameter holes.

2.10 Lower Boundary Condition.

The condition on the lower boundary was established prior to Experiment 1 by introducing water into the dry sand box with the constant level reservoir shown in Figure 16. The vertical advance of the capillary fringe is plotted for a period of 44 days in Figure 17. The elevations of the capillary fringe were determined from the visual contrast between wet and dry sand. The free surface in the constant level reservoir was maintained at Z = 2.5 centimeters before and during Experiments 1 through 5.

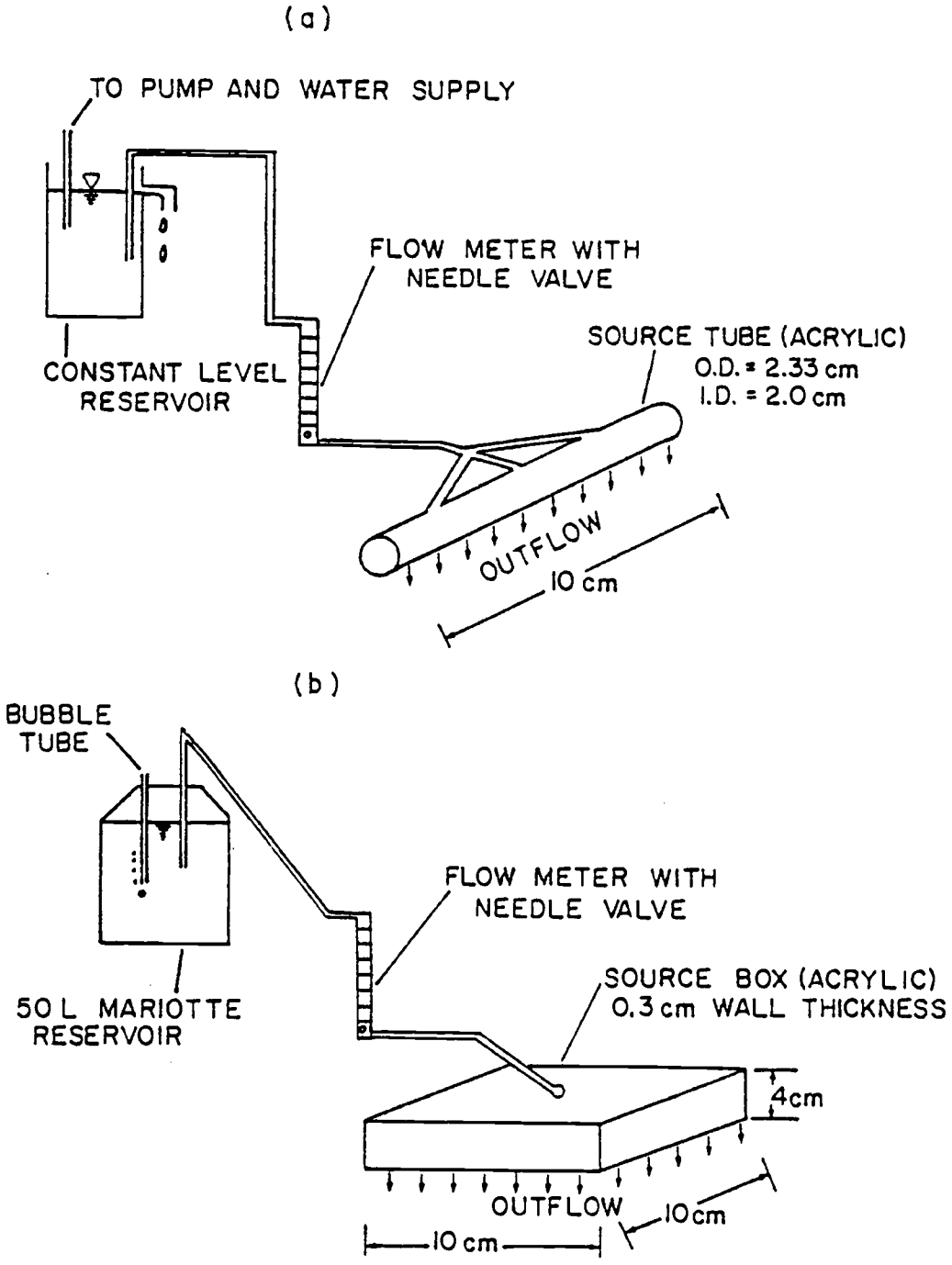

Figure 15. Schematic diagram of the source plumbing for (a) Experiments 1, 2, and 3 and (b) Experiments 4 and 5.

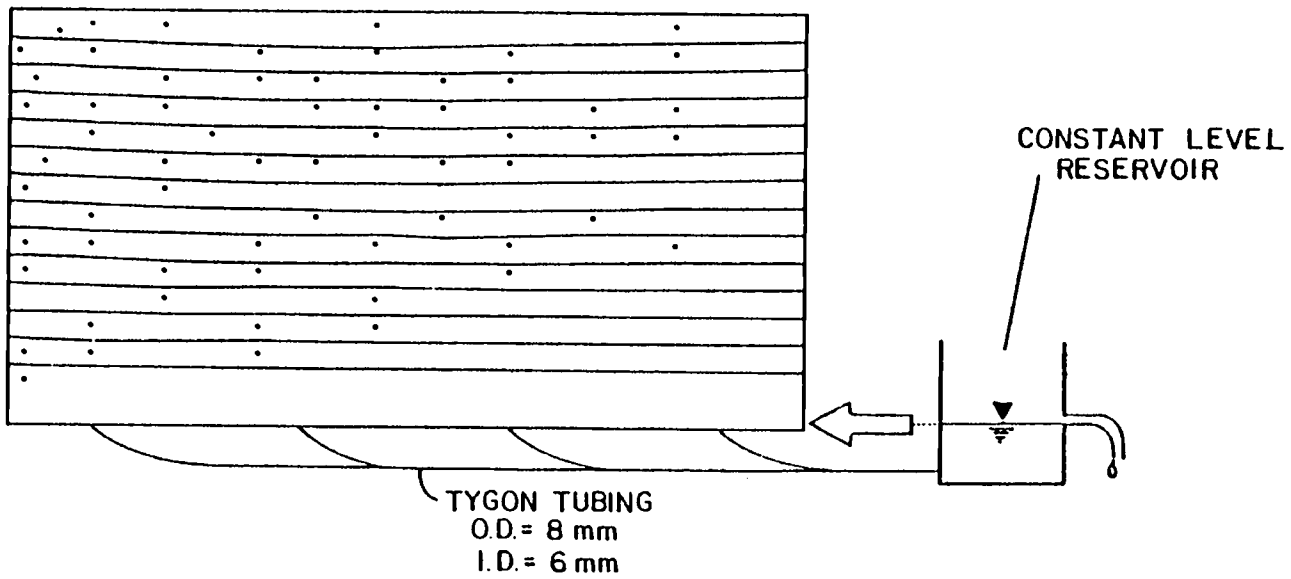

Figure 16. Design of the lower boundary. Free surface in reservoir is positioned 2.5 cm above the base of the sand box.

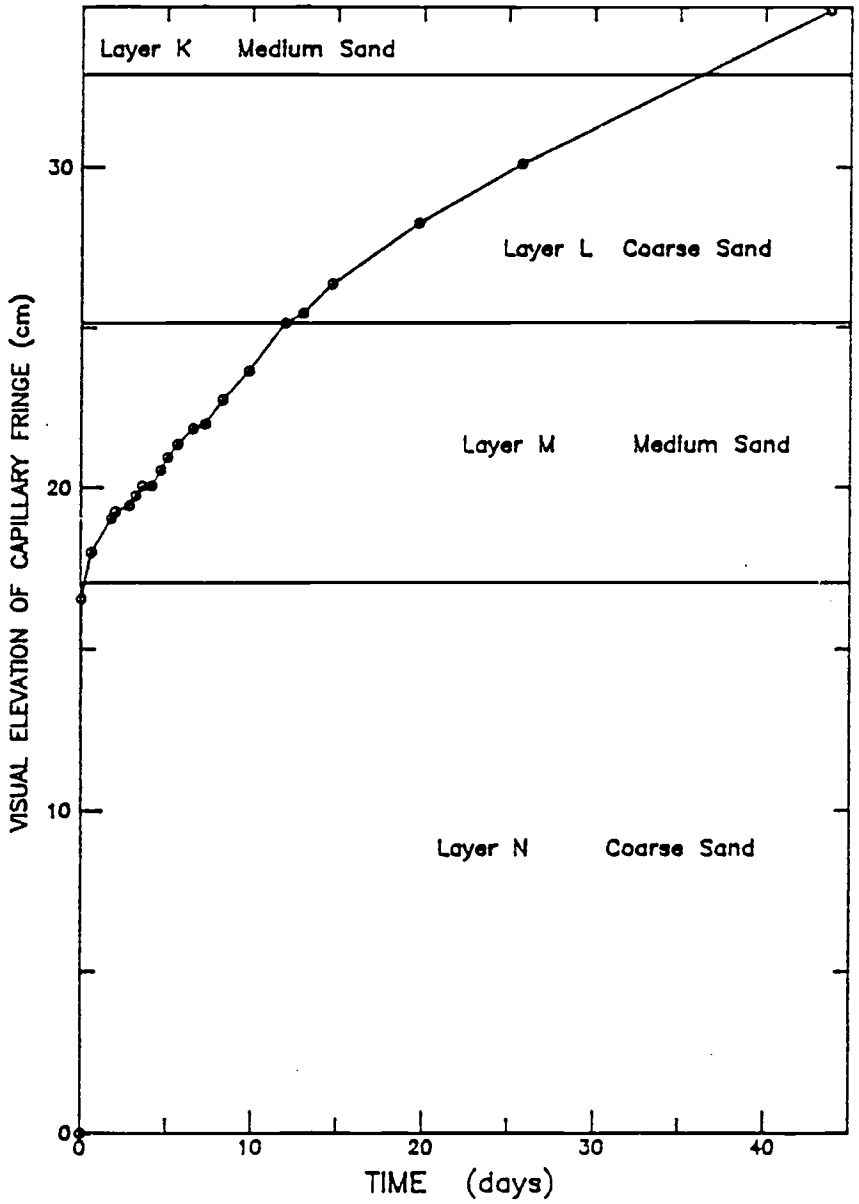

Figure 17. Average capillary fringe position as a function of time.

CHAPTER 3

DISCUSSION OF EXPERIMENTAL CONDITIONS AND RESULTS

This chapter describes the conditions and results for Experiments 1 through 5. The purpose of Experiment 1 was to: 1) observe the behavior of the wetting front during infiltration into the initially dry sand and 2) wet the entire flow domain so that all 62 tensiometers could be installed for tension measurement in subsequent experiments. Experiments 2, 3, 4, and 5 were conducted to obtain the tension head distribution for infiltration events subject to different boundary and initial conditions. The results are discussed both in the context of the physical flow behavior of each experiment and stochastic theory of Yeh et al. (1985a, b, c) and Mantoglou et al. (1987a, b, c). This chapter includes three sections which are: 1) Experiment 1, 2) Experiments 2 and 3, 3) Experiments 4 and 5, and 4) Comparison of Tension Head in Experiments 2, 3, 4, and 5.

3.1 Experiment 1.

The boundary conditions and infiltration-redistribution history for Experiment 1 is shown in Figures 18 and 19. The three infiltration - redistribution events for Experiment 1 are labeled 1A, 1B, and 1C. The stratified sand was air dry prior to Experiment 1A. Flux at the source was approximately 0.03 cm/s for the three infiltration events. This flux rate is approximately two fifths the K_{sat} value of 0.078 cm/s for layer A. Each tensiometer was inserted into the sand box after the wetting front had passed each port location (Figure 14). The tensiometer was pushed into a hole that was made by coring the wet sand with a 10.7 cm long x 0.95 cm O.D. cork borer. All 62 tensiometers were in place and operating prior to Experiment 2 (next section).

3.1.1 Infiltration-Redistribution Event 1A.

The position of the wetting front as a function of time is shown for the first

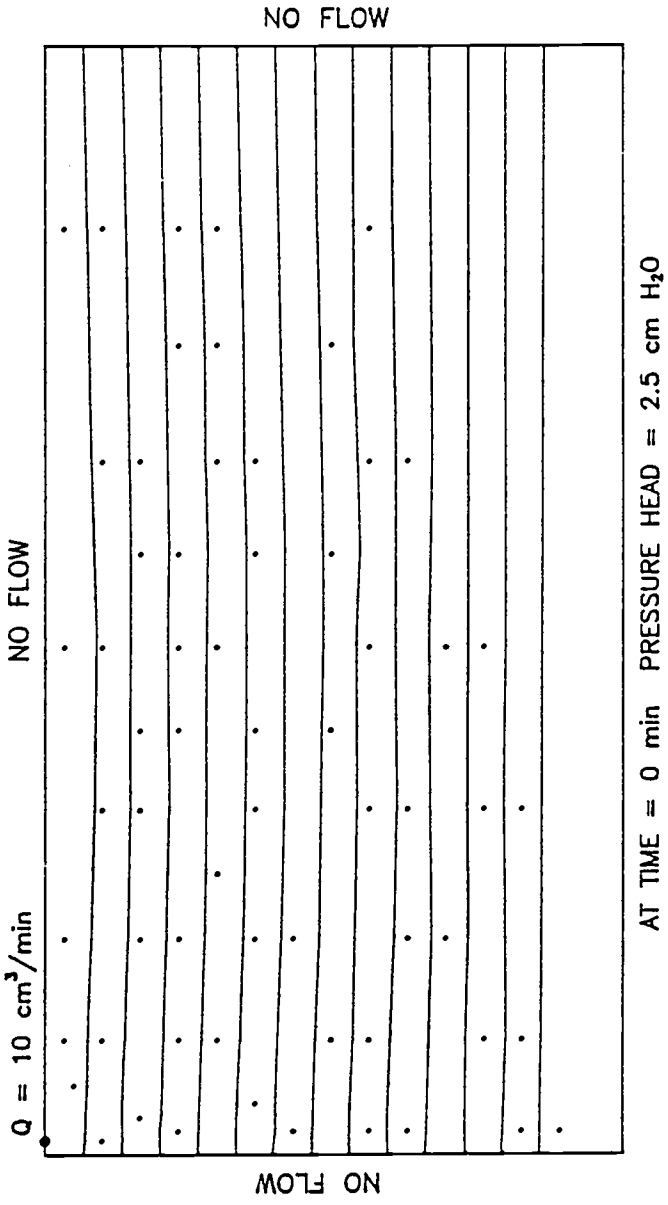

Figure 18. Boundary conditions for Experiment 1.

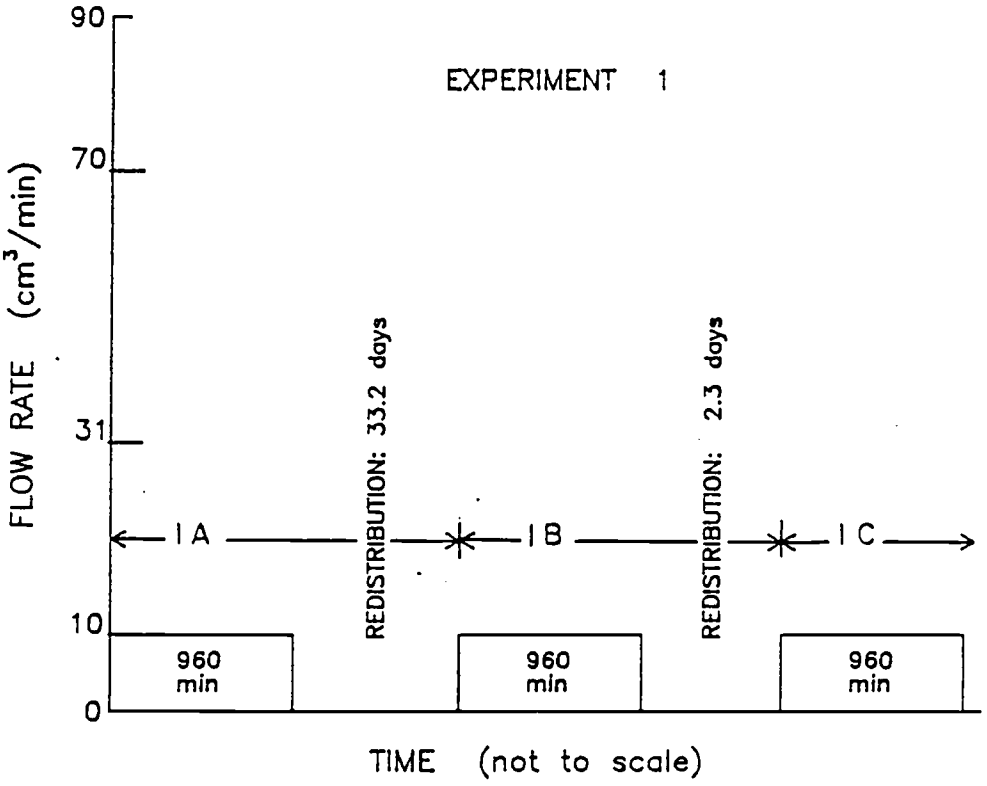

Figure 19. Infiltration - redistribution history for Experiment 1: Events 1A, 1B, and 1C.

12,460 minutes (8.65 days) of event 1A in Figure 20. The 10 cm^3/min point source was terminated at 960 minutes for event 1A. Two prominent features of the infiltration-redistribution event shown in Figure 18 are: a) the greater lateral flow versus vertical flow by an approximate ratio of five to one on the scale of the entire sand tank and b) the development and dissipation of wetting front instability (referred to as 'lobes' in this paper) in the vertical direction both below the source and in layers D and E. These lobes are on the order of 10 centimeters in the horizontal dimension.

The general lateral flow illustrated in Figure 20 is controlled by the integrated small-scale phenomena at the medium on coarse sand interface. The vertical rate of advance was significantly reduced or stopped as the wetting front reached the medium on coarse sand interface (see contour '10', Figure 20). Consequently, water flowed laterally within the medium sand due to the extremely small conductivity in the dry coarse sand. One could view this in terms of two products in which

$$K(\psi)_{lat}\ I_{lat} \quad >> \quad K(\psi)_{ver}\ I_{ver} \tag{7}$$

where $K(\psi)_{lat}$ and I_{lat} is the hydraulic conductivity and hydraulic gradient in the lateral direction, and $K(\psi)_{ver}$ and I_{ver} is the hydraulic conductivity and hydraulic gradient in the vertical direction at the interface. As the capillary tension head decreased at the interface, water filled the larger pores in the coarse sand and the wetting front advanced in the vertical direction (see contour '30', Figure 20).

This vertical advance of the wetting front across the interface implies a large increase in unsaturated hydraulic conductivity in the coarse sand within a small fixed volume centered on the interface. Figure 21 shows the possible change in unsaturated hydraulic conductivity for the medium and coarse sand as the tension

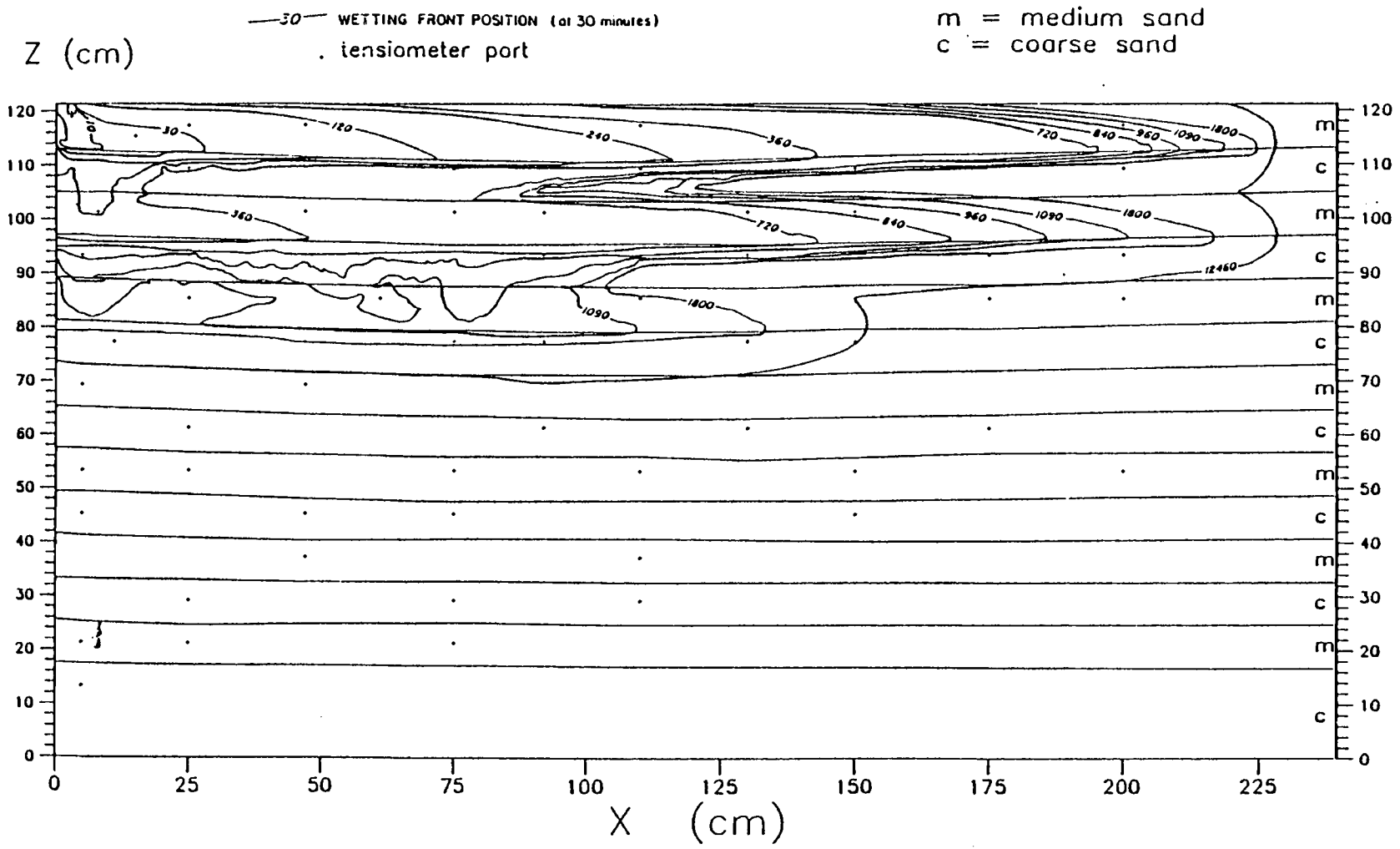

Figure 20. Wetting front postion for the first 12,460 minutes (8.65 days) of infiltration - redistribution event 1A.

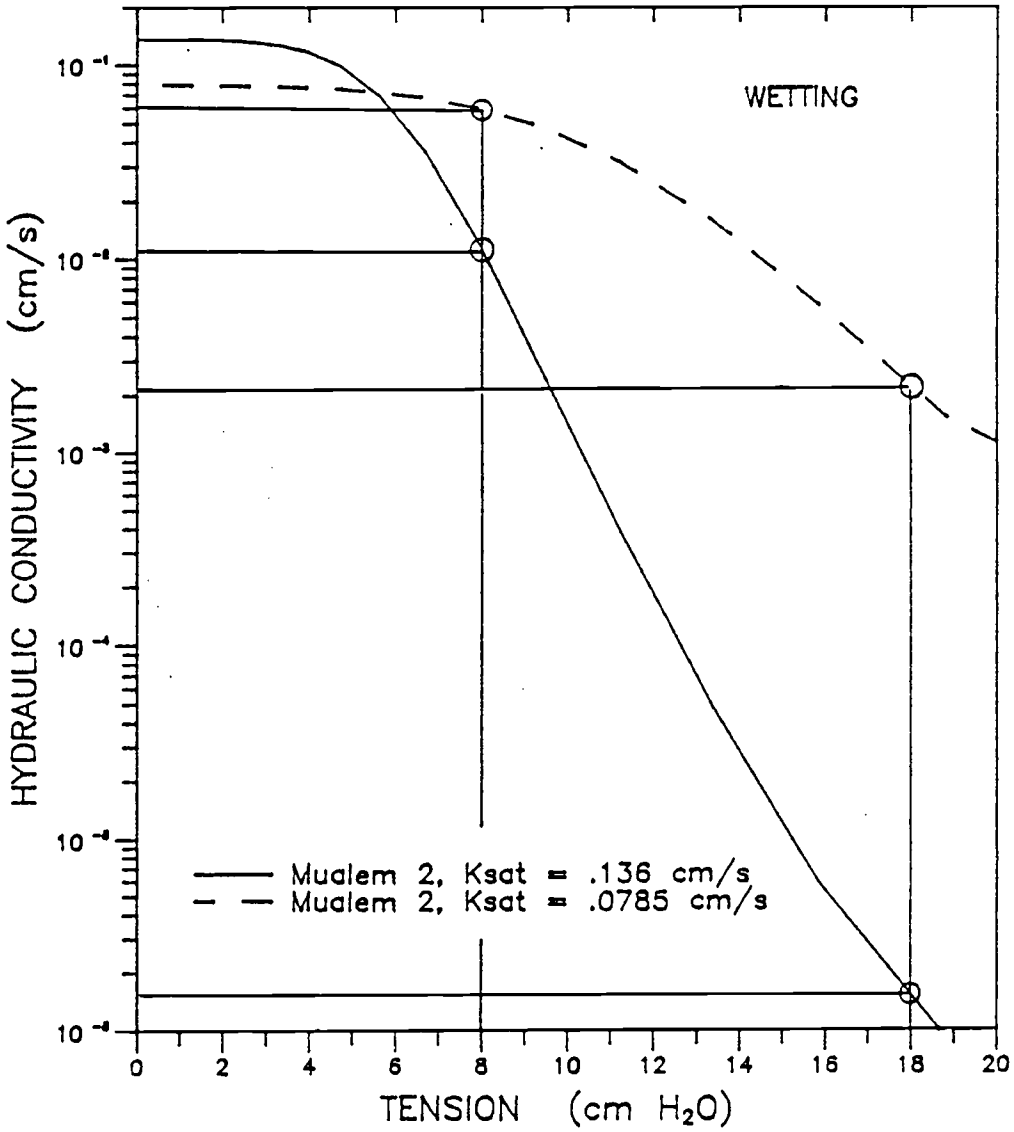

Figure 21. Predicted unsaturated hydraulic conductivity for the medium (dashed) and coarse (solid) sand: Wetting Cycle. Figure illustrates the possible change in conductivity at the interface between the two sands as the tension head decreases from 18 to eight centimeters of H_2O.

head at the interface decreases from 18 to 8 cm H_2O. Note the increase in conductivity of the coarse sand is approximately 10^4 from 18 to 8 cm H_2O compared to 10^1 for the conductivity of the medium sand. A decrease in tension head averaged over this volume would result in an increase in the effective vertical conductivty that is greater than the increase in the effective lateral conductivity. This small scale phenomena at the medium on coarse sand interface for event 1A implies the anisotropy changes from relatively large to small values as the tension head changes from relatively large to small values. This observation, while not validating large-scale saturation dependent anisotropy, does qualitatively support the flow characteristics embodied in saturation dependent anisotropy.

The second prominent feature mentioned above is the development and dissipation of the wetting lobes. One might expect to observe this phenomena below the infiltration source where water contents and hydraulic gradients should be relatively large. This is observed during the infiltration-redistribution event of Experiment 1A (Figure 20). The lobes below the source developed between t = 0 to 10 minutes, t = 120 to 360 minutes, and t = 720 to 1800 minutes. However, these three lobes were dissipated as they crossed the medium on coarse sand interface at approximately t = 10 minutes, t = 360 minutes, and t = 1800 minutes.

The region bounded by the top of layer D, the bottom of layer E, and 50 cm < X < 100 cm in Figure 20 shows the position of two lobes <u>not</u> below the infiltration source. The irregular shaped 840 minute front in layer D and the two lobes in layer E cannot be correlated with a perceptible sand heterogeneity within either of the two layers. However, the layer C (medium) - layer D (coarse) interface position shown in Figure 22 (vertical exaggeration: 8.1x) reaches a minimum at approximately X = 75 centimeters. Perhaps water accumulated at this location of minimum interface elevation and contributed to the development of the lobe at approximately X = 80 centimeters in layer E. The two lobes in layers D and E were also dampened as they cross the medium on coarse sand interface at t = 1800

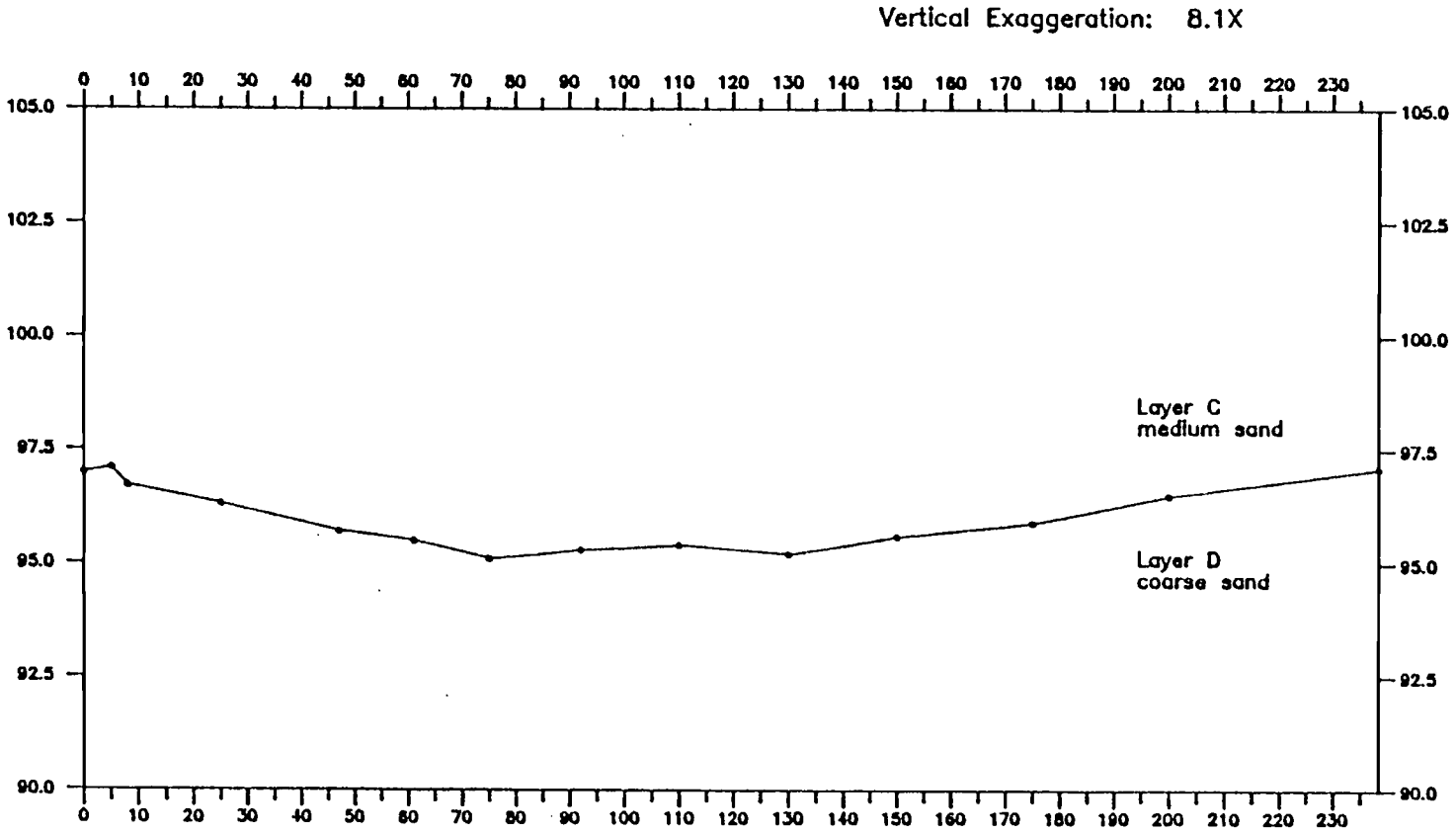

Figure 22. Interface position between layers C (medium sand) and D (coarse sand). Veritical exaggeration: 8.1x. Note the minimum point at approximately X = 75 cm.

minutes. In general, the initially dry stratified sand contributes to both the development of preferential flow paths in the lateral and vertical directions and the dissipation of preferential flow paths in the vertical direction.

3.1.2 Infiltration-Redistribution Event 1B.

The redistribution of event 1A was follow by the infiltration of event 1B (Figure 19). The wetted region in the sand tank prior to the infiltration of event 1B is outlined by the 46,845 minute (32.5 days since t = 0.0 of event 1A) wetting front in Figure 23. This figure also shows the wetting front position for event 1B at t = 660, 900, and 1200 minutes after the start of the 10 cm^3/min point source. The important feature in Figure 23 is the wetting front at the end of the infiltration period (t = 960 minutes, not drawn) for event 1B reached the edge of the sand tank in layers A and C (medium sand). This represents lateral advance of the wetting front of 30 and 55 centimeters greater than that observed at t = 960 minutes in layers A and C for infiltration event 1A.

The greater lateral advance for event 1B is perhaps counter- intuitive particularly with reference to the saturation dependent anisotropy concept. One might expect that since the system (the stratified sand) contained more water prior to infiltration event 1B compared to event 1A. then relatively large effective vertical conductivities would facilitate predominately vertical advance of the wetting front. Yet, a substantial lateral advance of the wetting front is observed during event 1B (Figure 23).

A possible mechanism for enhanced lateral flow in a hypothetical stratified domain is depicted in Figure 24. An infiltration event wets a relatively dry sequence of fine and coarse layers. Flow is both lateral and vertical (Figure 24a). The source stops and a long redistribution event starts. Water diffuses in all directions, but gravity drainage is significant. As the coarse layers drain they impede water draining from the fine layers. Consequently, water accumulates at the base of the fine layers. The contrast in the conductivity at the fine on coarse layer

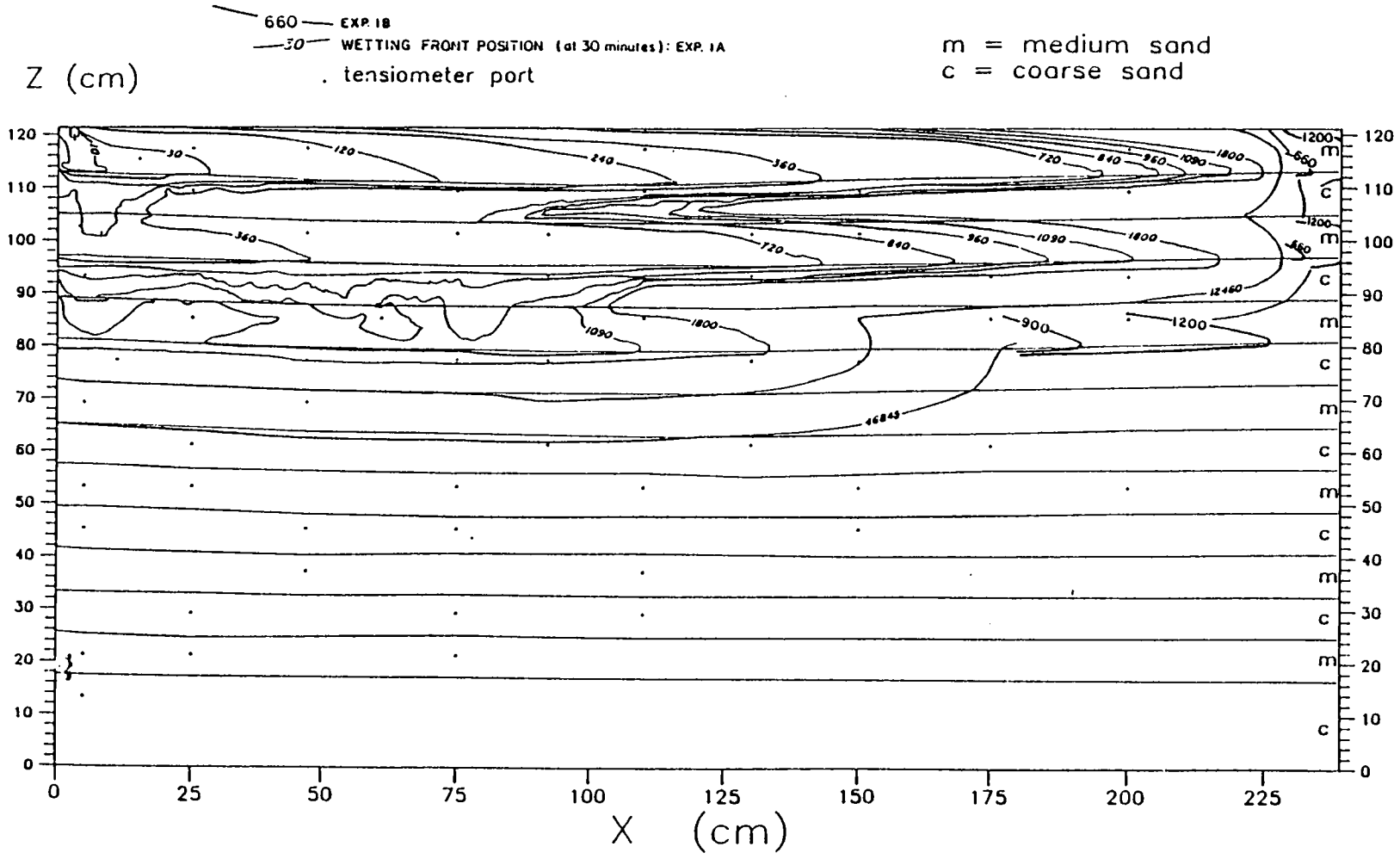

Figure 23. Wetting front positions as shown in Figure 20 and front position at 46,845 minutes (32.5 days) after start of event 1A. Figure also shows the wetting front position a t = 660, 900, and 1200 minutes after start of event 1B.

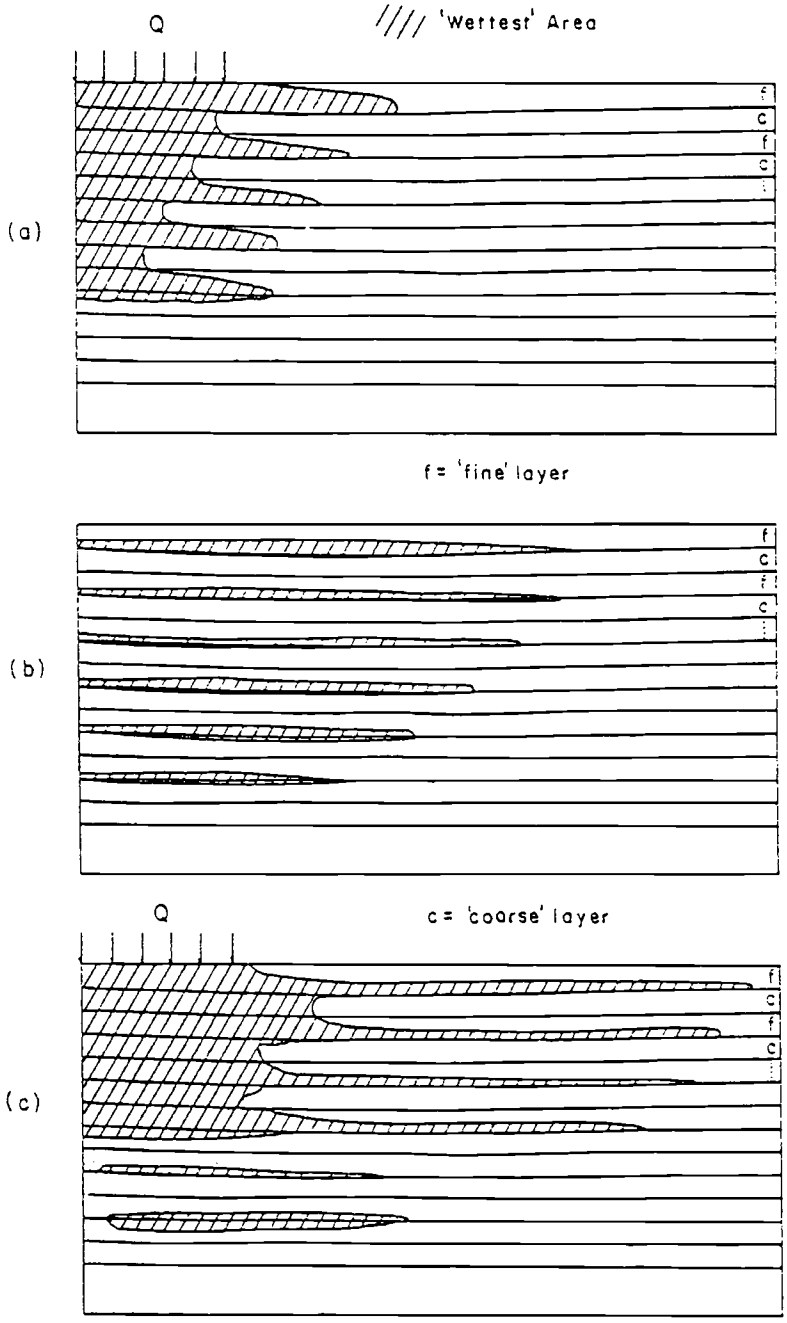

Figure 24. Schematic diagram a of mechanism for enhanced lateral flow resulting from an (a) infiltration - (b) redistribution - (c) infiltration event in a layered porous media.

interface greatly increases (Figure 24b). A second infiltration event starts and the relatively wet fine layers conduct a large percentage of the infiltrated water in the lateral direction (Figure 24c).

The scenario above is similar to the water content heterogeneity suggested by McCord et al. (1988) to explain the downslope movement of the water in an apparently homogeneous dune sand. These authors depict a scenario in which a stochastic rainfall event produces a wet 'layer' below a sloping land surface. During redistribution the 'layer' moves in the vertical direction. A subsequent rainfall event causes near surface vertical infiltration follow by downslope movement of water in the highly conductive wet 'layer'. This same phenomena is likely to occur during event 1B of Experiment 1. However, the sand stratification likely controls the formation of a wet 'layer' above the medium on coarse sand interface.

3.2 Experiments 2 and 3.

The boundary conditions for Experiments 2 and 3 are shown in Figure 25. These two experiments were separated in time by a 810 minute redistribution interval (Figure 26). The purpose of the redistribution was to conduct two experiments with the same boundary conditions but with different initial conditions. An estimate of the source flux rate is 0.103 cm/s. K_{sat} for the medium sand is 0.078 cm/s.

The initial tension profiles for Experiments 2 and 3 are shown in Figure 28a. (Refer to Figure 27 for the transect location of the tension and water content profiles shown in Figures 28, 29, 34, and 35.). The dashed lines connecting the data point labels in Figure 28 are included as a visual aid and are not intended to represent the tension distribution between two measured tension values.

The tension profiles from Experiments 2 and 3 at 540 minutes are shown in Figure 28b. The transient readings shown in Figure 28b (and Figures 29, 34, and 35) are attributed to a real change in the soil-tension around the tensiometer and/or the transient response of the tensiometer-manometer instrument. Figure 28b shows that

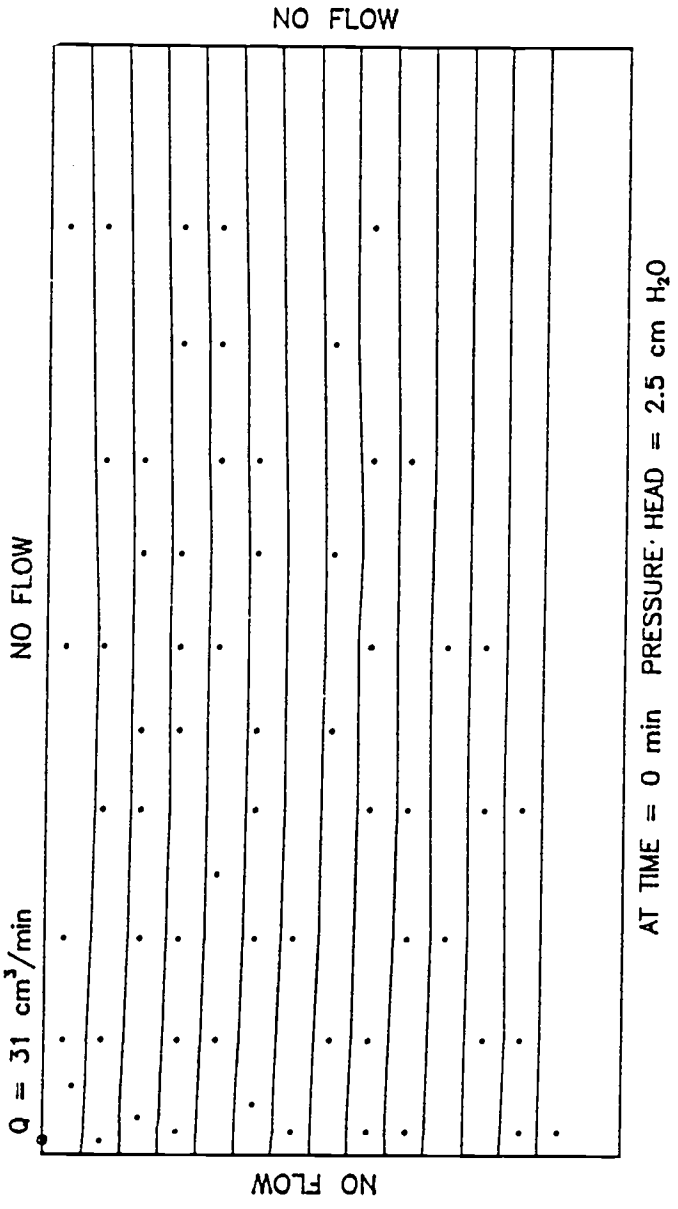

Figure 25. Boundary conditions for Experiments 2 and 3.

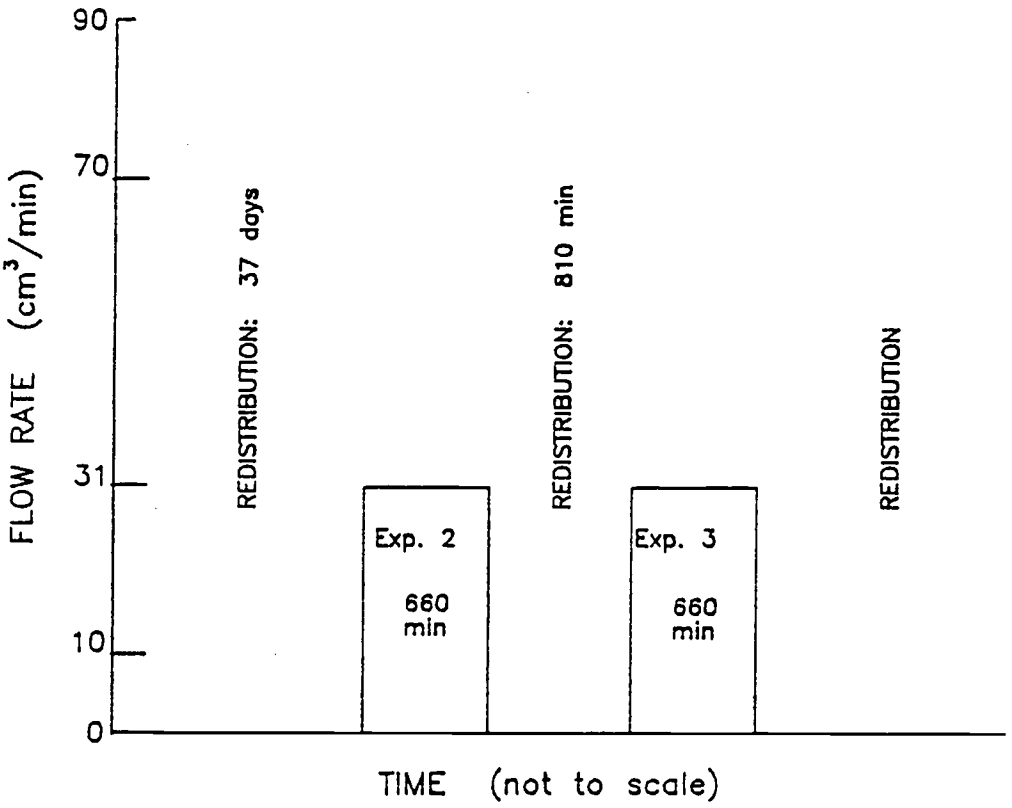

Figure 26. Infiltration - redistribution history for Experiments 2 and 3.

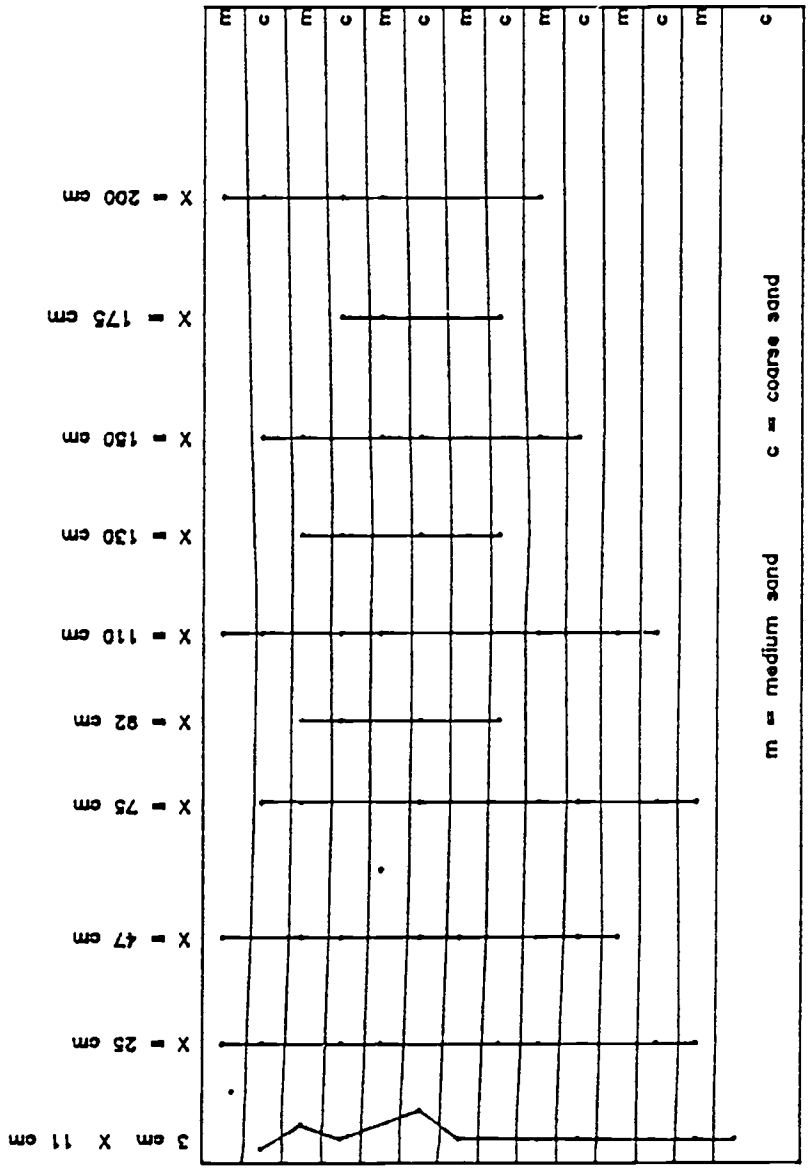

Figure 27. Transect locations for tension head and water content profiles shown in Figures 28, 29, 34, 35, and 38.

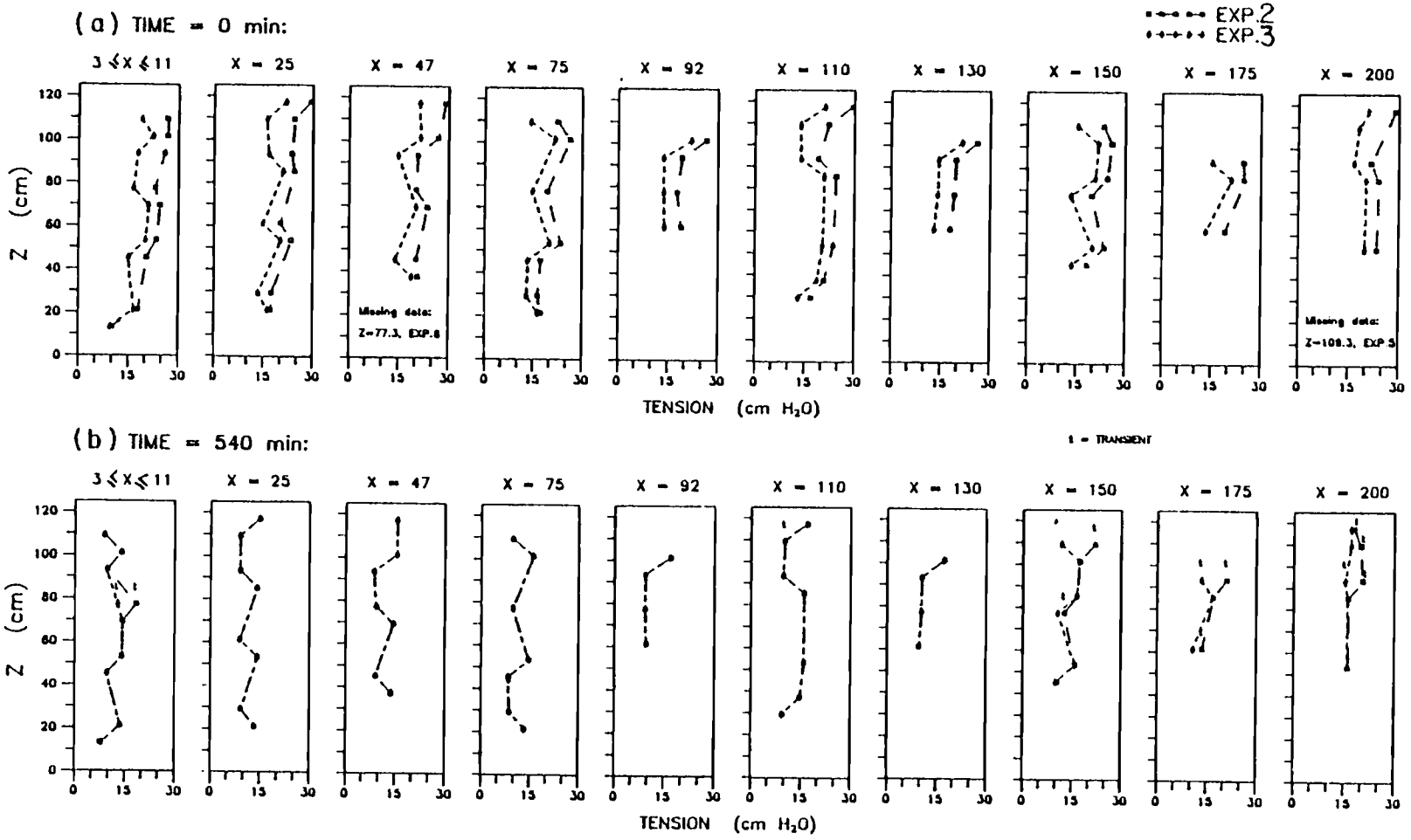

Figure 28. Measured tension head profiles for Experiments 2 and 3 at (a) t = 0.0 minutes and (b) 540 minutes.

the tension profiles are nearly identical for Experiments 2 and 3 in spite of the difference in initial tension profiles (Figure 28a). These results show that the system is not sensitive to the initial tension conditions of Experiments 2 and 3.

The initial condition water content profiles for Experiments 2 and 3 are shown in Figure 29a. Water content at each tensiometer is inferred from the water content-tension head wetting curves that characterize the medium and coarse sands (Figure 5). Assuming that the water content profiles in Figures 29a and 29b approximate the in situ water content for Experiments 2 and 3, then Figure 29b shows the system is not sensitive to the small but different initial water content conditions in Experiment 2 and Experiment 3.

Figures 30 and 31 are hand contoured plots of the initial and 540 minute capillary tension head distributions for Experiment 2. In general, the 17 and 13 cm H_2O closed contours in Figure 30 indicate the tension head and water content distribution is controlled by the concave-up shape of the layer interfaces. The contours in Figure 31 indicate that lateral tension head gradients exist in the medium sand.

A statistical summary of the tension head values for Experiment 2 and 3 is presented in Table 5. These statistics include tension head measurements from tensiometers that were at steady-state at $t = 0$ and 540 minutes. Table 5 shows the larger mean tension head (drier sand) for Experiments 2 and 3 correspond to larger variances compared to the mean and variances at 540 minutes. This supports the stochastic result of Yeh et al. (1985a and b) that indicates an increase in the mean capillary tension head is proportional to an increase in the tension head variance.

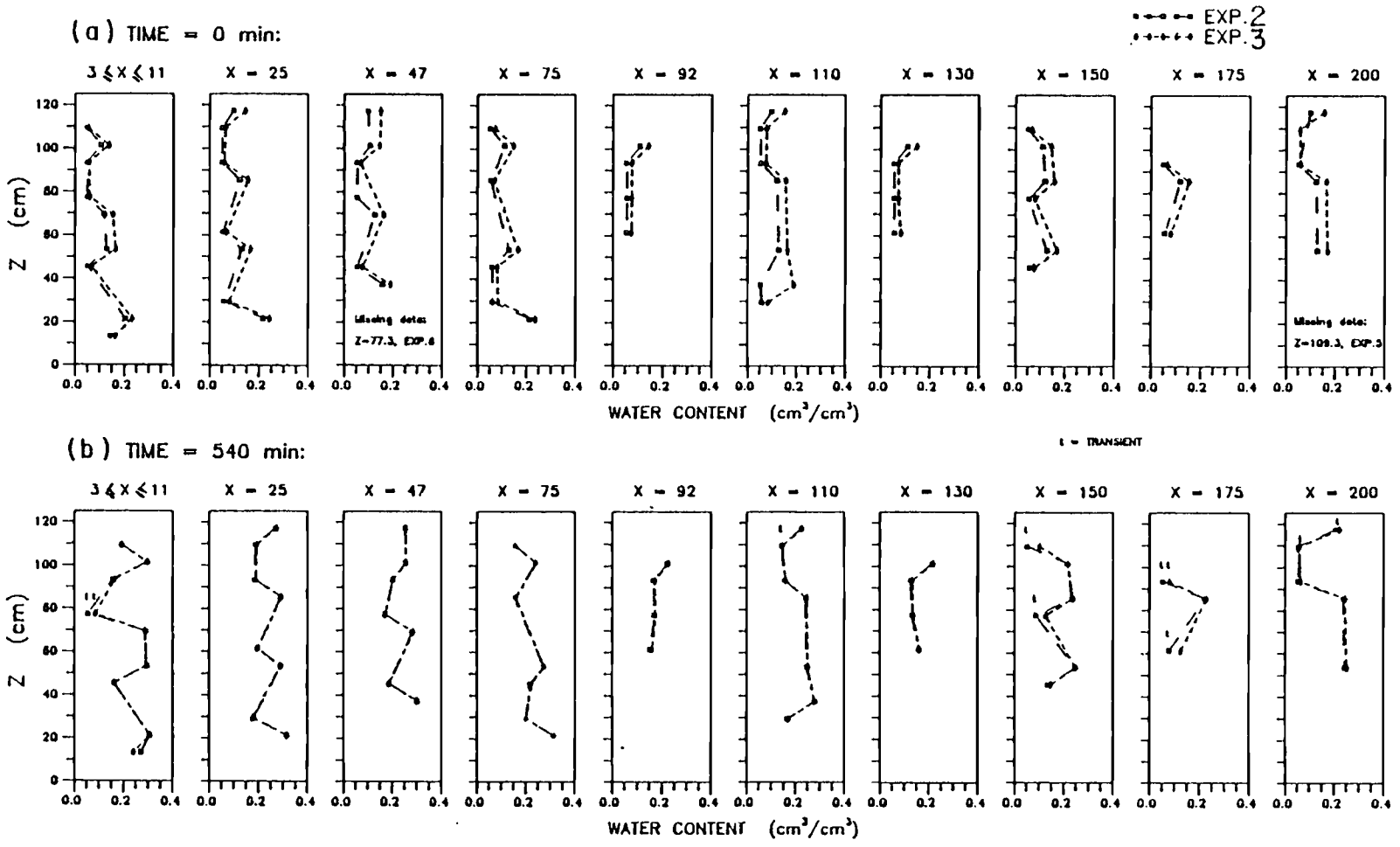

Figure 29. Inferred water content profiles for Experiments 2 and 3 at (a) t = 0.0 minutes and (b) 540 minutes.

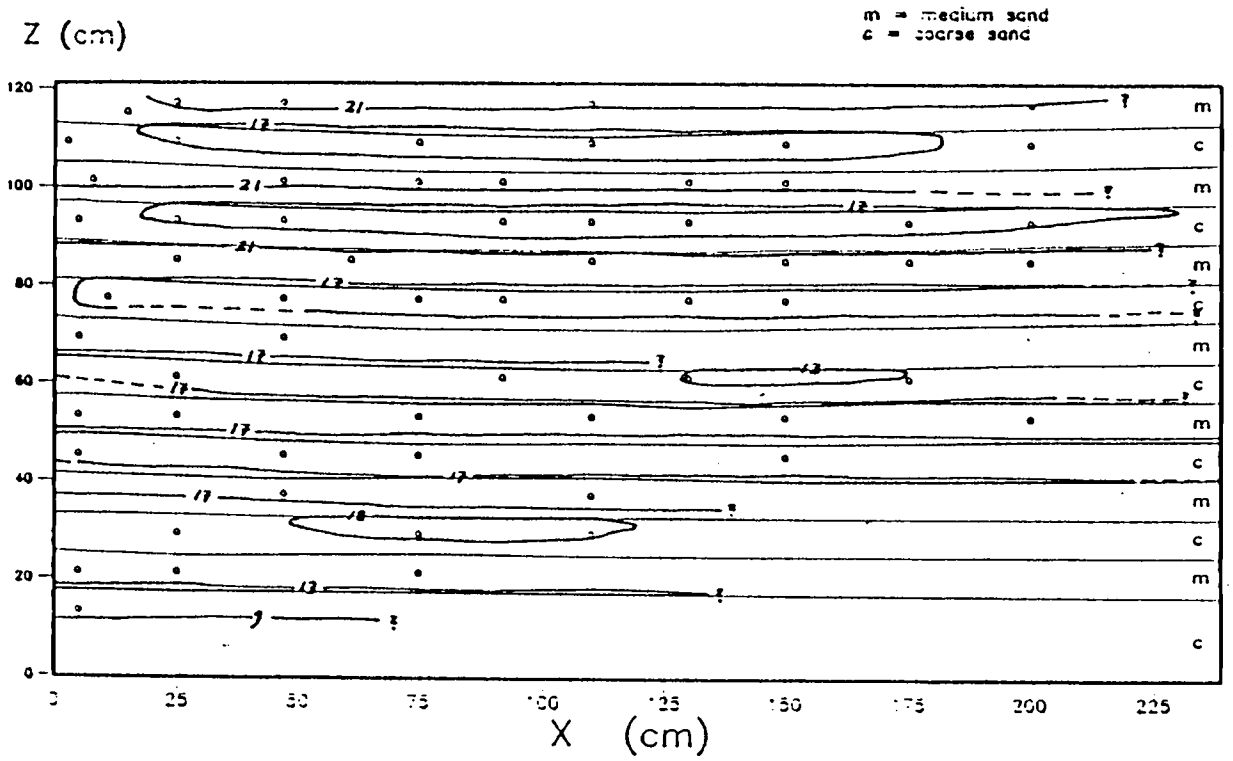

Figure 30. Contour plot of tension head (cm H_2O) for Experiment 2 at t = 0.0 minutes.

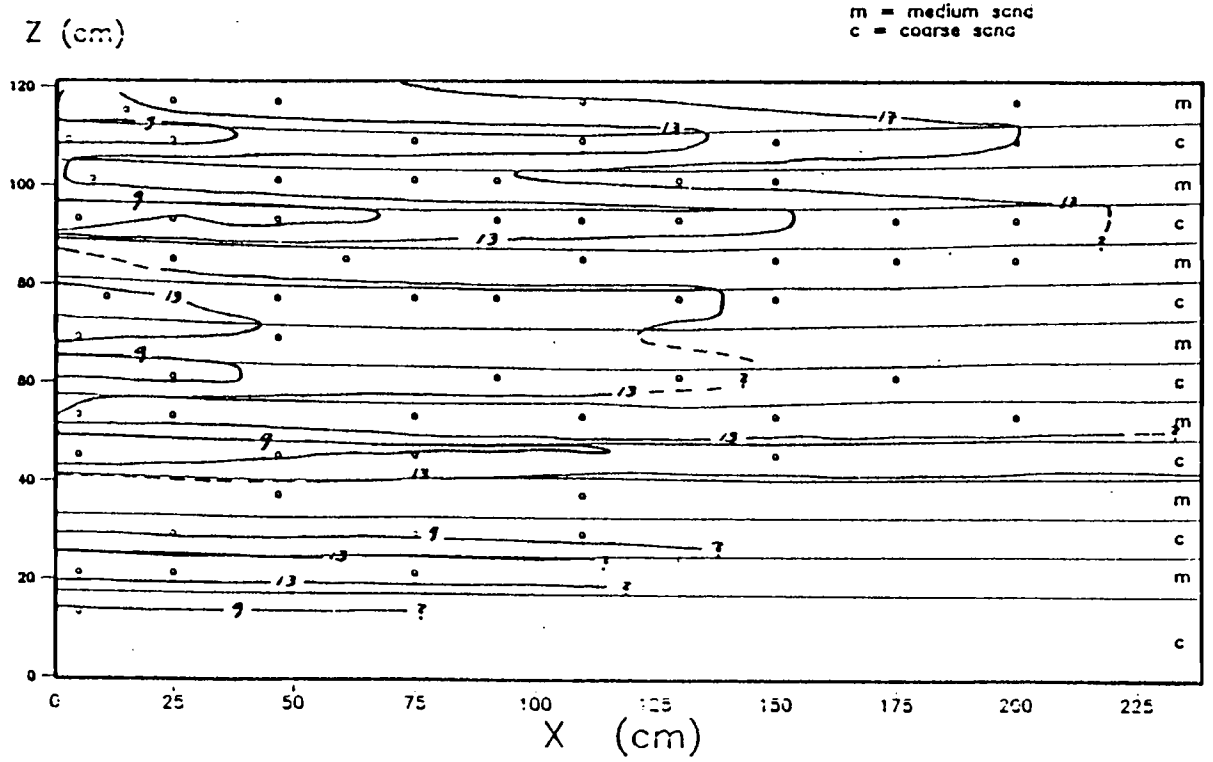

Figure 31. Contour plot of tension head (cm H_2O) for Experiment 2 at t = 540 minutes.

Table 5: Statistics of tension head measurements for medium and coarse sands.

	TIME = 0.0 min.	TIME = 540 min.
	Exp. 2	
n_{ten}	53 tensiometers	
ψ	22.12	12.53
s^2	15.51	9.76
ν	0.178	0.249
	Exp. 3	
n_{ten}	58 tensiometers	
ψ	17.42	12.56
s^2	11.56	9.51
ν	0.195	0.245

n_{ten} = number of samples (tensiometers)
ψ = mean tension head in cm H_2O
s^2 = variance of the tension head measurements
ν = coefficient of variation

3.3 Experiments 4 and 5.

The boundary conditions for Experiments 4 and 5 are shown in Figure 32. In contrast to Experiments 2 and 3, the source for Experiments 4 and 5 was a channel in which water flowed from the source box and across the base of the channel. The flow rate for Experiments 4 and 5 was 70 cm^3/min, approximately 2.3 times greater than the flow rate for Experiments 2 and 3 (Figure 26 and 33). Again, the purpose for the 1370 minute redistribution interval between Experiments 4 and 5 was to conduct two experiments with the same boundary conditions but with different initial conditions. Flux across the channel base is approximately 0.013 cm/s. The initial tension profiles are shown in Figure 34a.

Tension profiles from Experiments 4 and 5 at 240 minutes are shown in Figure 34b. The tension values for Experiments 4 and 5 are identical with the exception of the transient measurements. The steady-state tension profiles in Experiments 4 and 5 at 240 minutes show that this system is not sensitive to the different initial tension conditions shown in Figure 32a.

The initial water content profiles for Experiments 4 and 5 are shown in Figure 35a. Water content at each tensiometer was inferred from the tension-water content wetting curves that characterize the medium and coarse sands (Figure 5). Assuming that the water content profiles in Figures 35a and 35b approximate the in situ water content for Experiments 4 and 5, then Figure 35b illustrates that the system is not sensitive to the small but different initial water content conditions in Experiment 4 and Experiment 5.

Figures 36 and 37 are hand contoured plots of the initial and 240 minute capillary tension head distributions for Experiment 4. In general, the 17 cm H_2O closed contours in Figure 36 indicate the tension head and water content distribution is controlled by the concave-up shape of the layer interfaces. The contours in Figure 37 indicate that lateral tension head gradients exist in the medium sand. The highly irregular shape of the contours in Figure 37 suggest that a two- dimensional

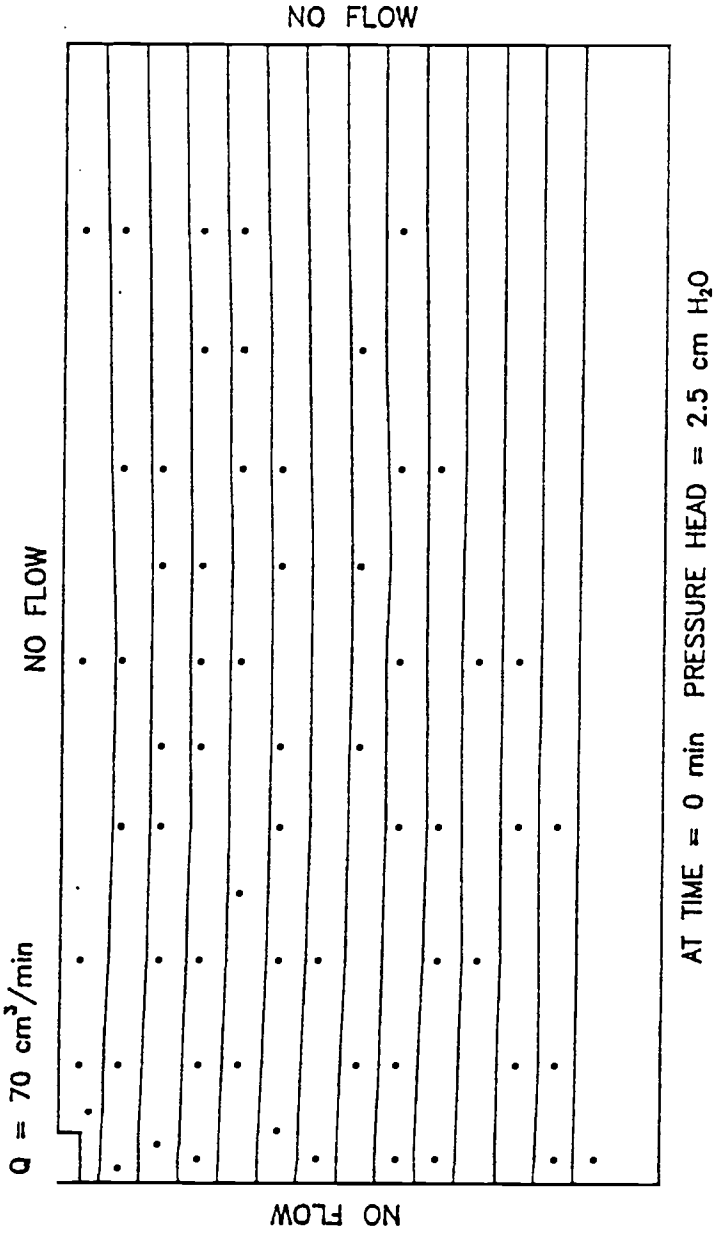

Figure 32. Boundary conditions for Experiments 4 and 5.

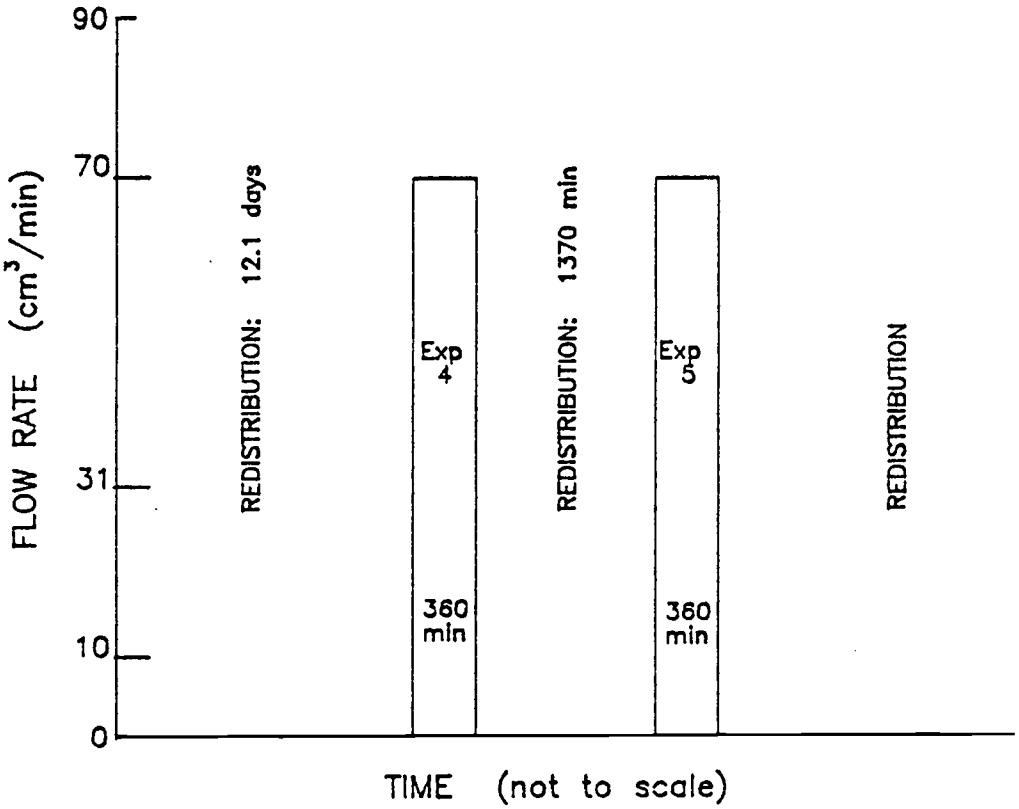

Figure 33. Infiltration - redistribution history for Experiments 4 and 5.

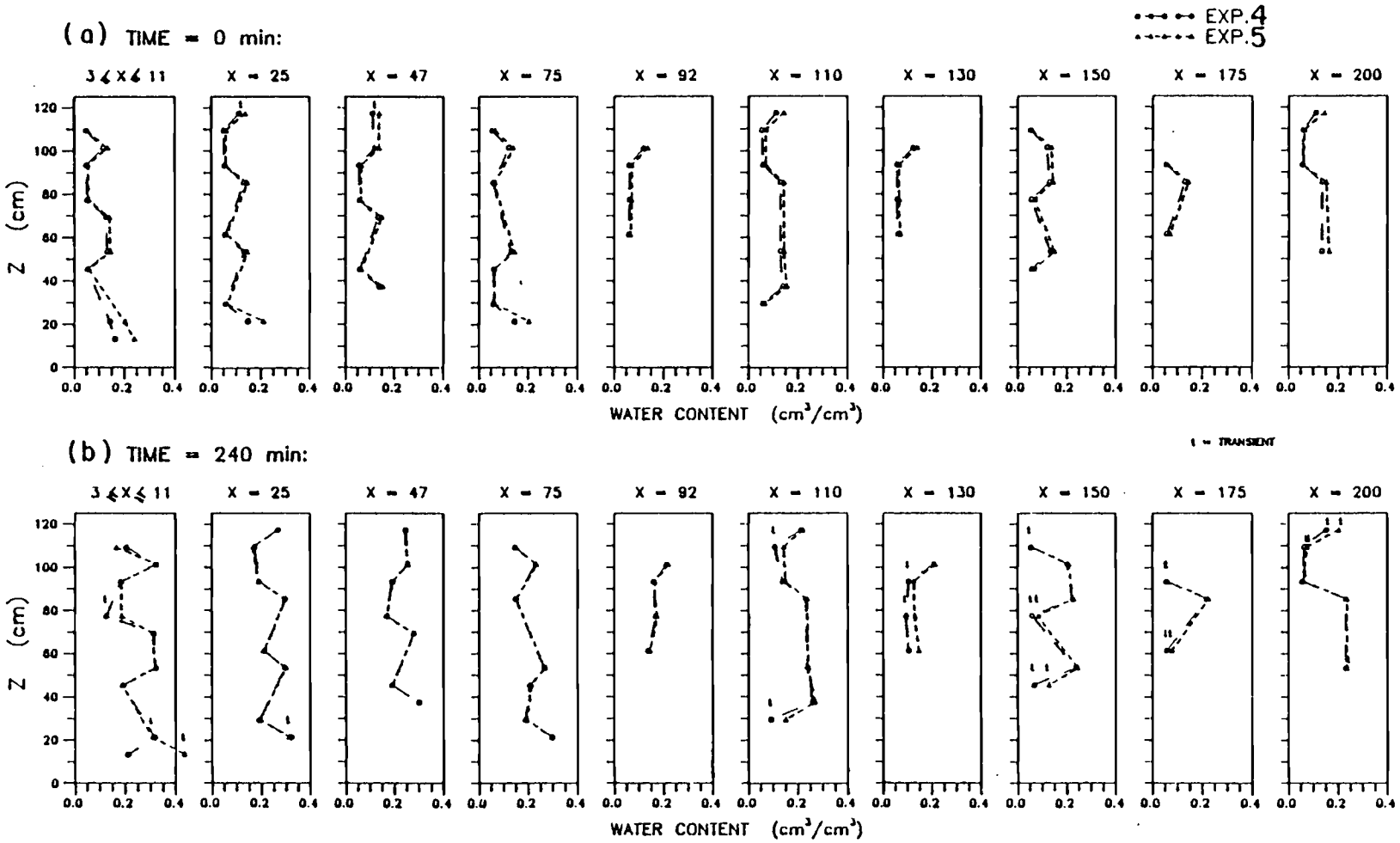

Figure 34. Measured tension head profiles for Experiments 4 and 5 at (a) t = 0.0 minutes and (b) 240 minutes.

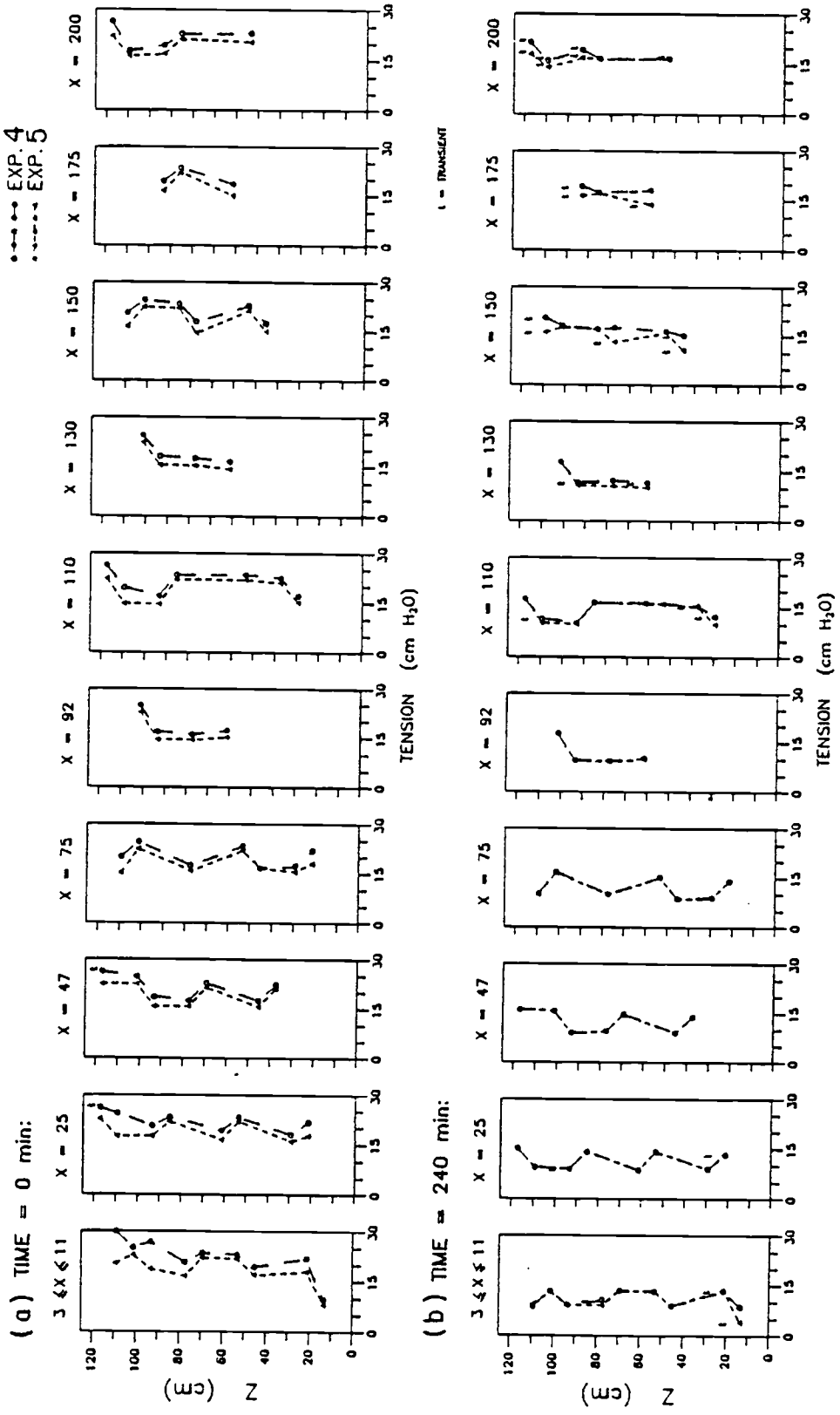

Figure 35. Inferred water content profiles for Experiments 4 and 5 at (a) t = 0.0 minutes and (b) 240 minutes.

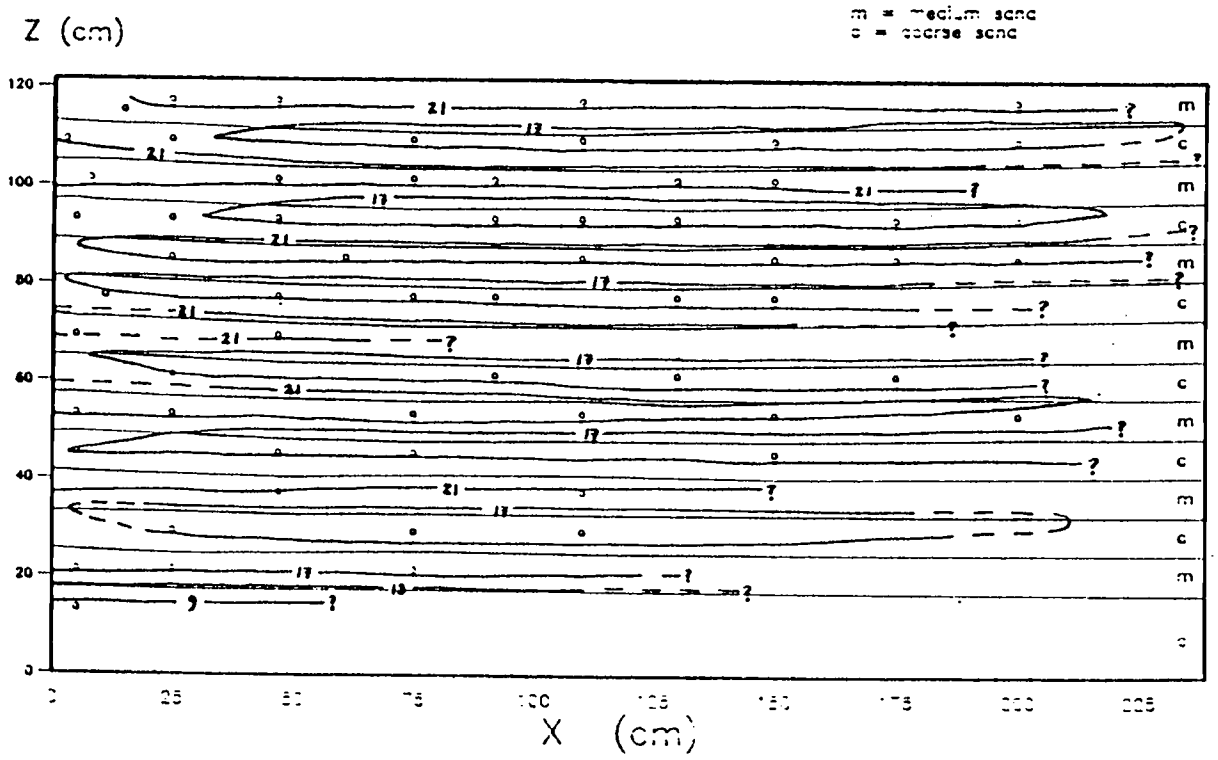

Figure 36. Contour plot of tension head (cm H_2O) for Experiment 5 at t = 0.0 minutes.

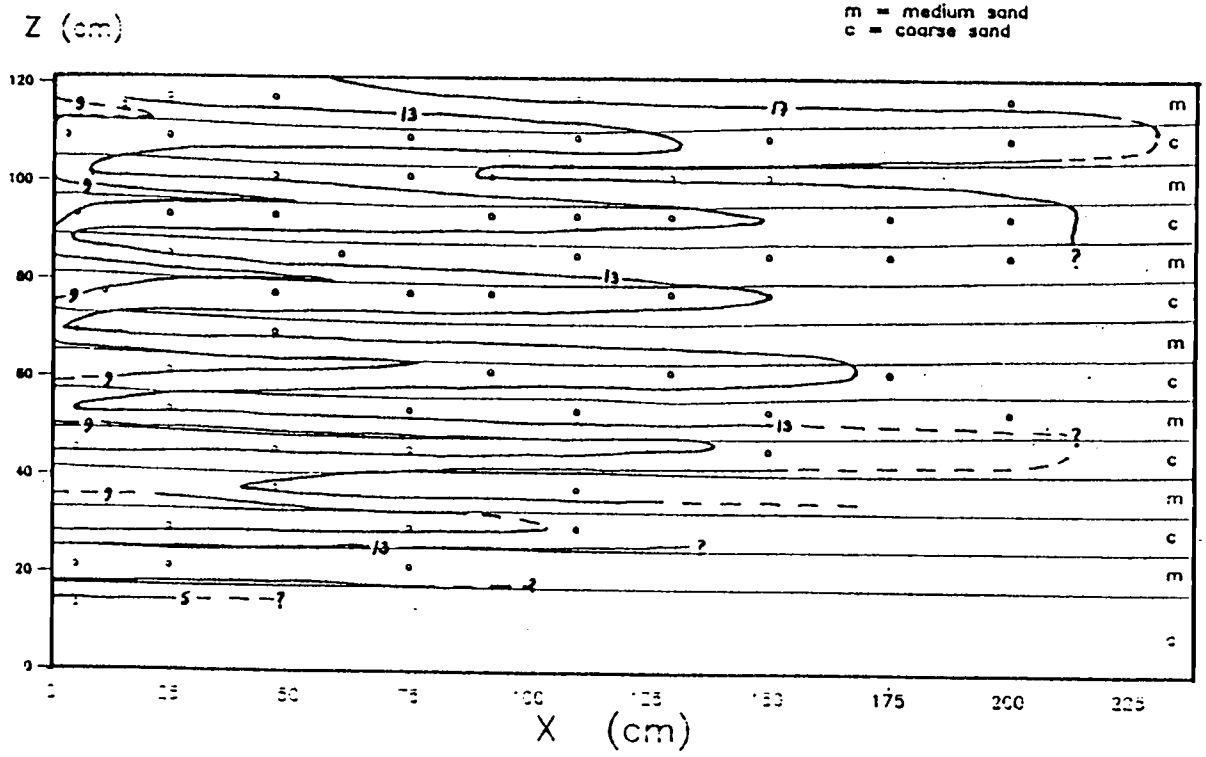

Figure 37. Contour plot of tension head (cm H_2O) for Experiment 5 at t = 240 minutes.

homogeneous and istropic model would not accurately represent the tension head distribution for Experiment 4. One could generalize this statement to the five sand tank experiments.

A statistical summary of the tension head values for Experiment 4 and 5 is presented in Table 6. These statistics include tension head measurements from tensiometers that were at steady state at t = 0 and 240 minutes. Table 6 shows the larger mean tension head (drier sand) for Experiment 4 corresponds to a larger variance compared to the mean and variance at 240 minutes. However, this is <u>not</u> true for Experiment 5.

Table 6: Statistics of tension measurements for medium and coarse sands.

	TIME = 0.0 min.	TIME = 240 min.
	Exp. 4	
n_{ten}	44 tensiometers	
ψ	21.47	12.76
s^2	13.47	11.35
ν	0.171	0.264
	Exp. 5	
n_{ten}	49 tensiometers	
ψ	18.97	12.57
s^2	10.06	10.05
ν	0.167	0.252

n_{ten} = number of samples (tensiometers)
ψ = mean tension head in cm H_2O
s^2 = variance of the tension head
ν = coefficient of variation

3.4 Comparison of Tension Head in Experiments 2, 3, 4, and 5.

Figure 38 compares the tension profiles of Experiments 2, 3, 4, and 5. Recall that the source for Experiments 2 and 3 was a point source and that the source for Experiments 4 and 5 was a channel source (Figures 25 and 32). The total flow rate was 31 cm^3/min for Experiments 2 and 3, and was 70 cm^3/min for Experiments 4 and 5 (Figures 26 and 33). The tension profiles shown in Figure 38 illustrate that the soil-water tension values at each tensiometer location are nearly identical regardless of the source geometry and source flow rates used in Experiments 2 and 3 versus Experiments 4 and 5.

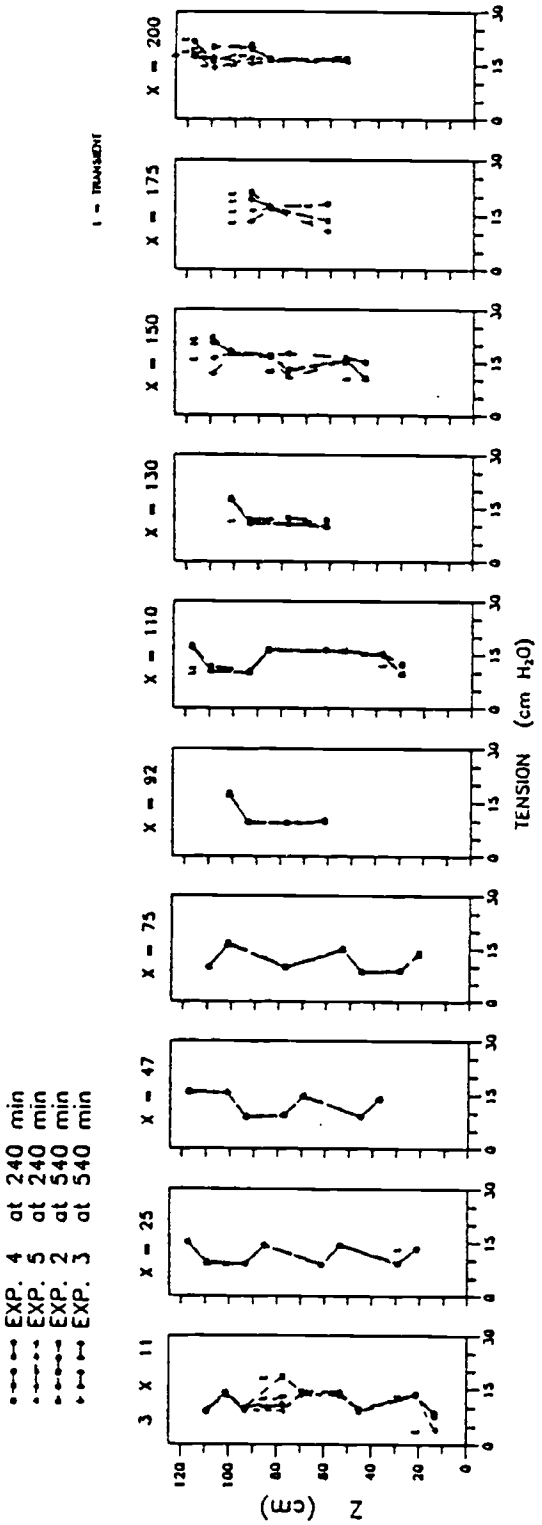

Figure 38. Comparison of tension head profiles (cm H_2O) for Experiments 2 and 3 at 240 minutes and Experiments 4 and 5 at 540 minutes.

CHAPTER 4

CONCLUSION

The five laboratory experiments show the stratified sand strongly influences the flow of water during infiltration and the capillary tension head distribution behind the wetting front. In particular, the layering facilitates the development and dissapation of preferential flow paths during infiltration into dry sand. The wetting front profiles of the infiltration - redistribution - infiltration of Experiment 1 (events 1A and 1B) suggest that water content heterogeneity (McCord et al., 1988) may be an important mechanism for increasing the lateral movement of water in layered porous media.

Experiments 2, 3, and 4 support the stochastic theory of Yeh et al. (1985a and b) that an increase in the variance of the capillary tension is proportional to an increase in the mean tension head. The wetting front behavior in Experiment 1 qualitatively supports the physical principles of the saturation dependent anisotropy concept. However, accurate mapping of the flux distribution and more tension head measurements are necessary to rigorously test saturation dependent anisotropy.

REFERENCES

Burdine, N. T., Relative permeability calculation from size distribution data, Trans. AIME, 198, 71-78, 1953.

Carvallo, H. O., D. K. Cassel, J. Hammond, and A. Bauer, Spatial variability of in situ unsaturated hydraulic conductivity of Maddock Sandy loam, Soil Sci., 121(1), 1-8, 1976.

Freeze, R. A. and J. A. Cherry, Groundwater, Prentice-Hall, Inc., 335-336, 1979.

Gardner W. H., film entitled "Water Movement in Soil", available from the Agronomy Club, Washington State Univ., Pullman, Washington, date unknown.

Mantoglou, A. and L. W. Gelhar, Stochastic modeling of large-scale transient unsaturated flow systems, Water Resour. Res., 23(1), 37-46, 1987a.

Mantoglou, A. and L. W. Gelhar, Capillary tension head variance, mean soil moisture content, and effective specific sil moisture capacity of transient unsaturated flow in stratified soils, Water Resour. Res., 23(1), 47-56, 1987b.

Mantoglou, A. and L. W. Gelhar, Effective hydraulic conductivities of transient unsaturated flow in stratified soils, Water Resour. Res., 23(1), 57-68, 1987c.

McCord, J. T., D. B. Stephens, and J. L. Wilson, Field-scale unsaturated flow and transport in a sloping uniform porous medium: field experiments and modeling considerations, Internat. Conf. and Workshop on the Validation of Flow and Transport Models for the Unsat. Zone, p. 256-267, eds. P. J. Wierenga and D. Bachelet, Ruidoso, New Mexico, May 22-25, 1988.

McKee, C. R. and A. C. Bumb, A three-dimensional analytical model to aid in selecting monitoring locations in the vadose zone, Ground Water Monitoring Review, 8(2), 124-136, Spring 1988.

Mualem, Y., A new model for predicting the hydraulic conductivity of unsaturated porous media, Water Resour. Res., 12(3), 513-522.

Murphy E. C., A. E. Kehew, G. H. Groenewold, and W. A. Beal, Leachate generated by an oil-and-gas brine pond site in North Dakota, Ground Water, 26(1), 31-38, 1988.

Nielson, D. R., J. W. Biggar, and K. T. Erh, Spatial variability of field measured soil-water properties, Hilgardia, 42(7), 215-260, 1973.

REFERENCES (continued)

Palmquist, W. N. and A. I. Johnson, Vadose flow in layered and nonlayered materials, U.S.G.S. Prof. Paper 450-C, C142-C143, 1962.

Philip, J. R., Theory of infiltration, Adv. in Hydrosci., ed. V. T. Chow, Academic Press, 5, 215-296.

Stephens, D. B., A. M. Parsons, E. D. Mattson, K. Black, K. Flanigan, R. S. Bowman, and W. B. Cox, A field experiment of three-dimensional flow and transport in a stratified soil, Internat. Conf. and Workshop on the Validation of Flow and Transport Models for the Unsat. Zone, p. 401-413, eds. P. J. Wierenga and D. Bachelet, Ruidoso, New Mexico, May 22-25, 1988.

Trauntwein, S. J., D. E. Daniel, and H. W. Cooper, Case history study of water flow through unsaturated soil, in The Role of the Unsaturated Zone in Radioactive Hazardous Waste Disposal, eds. T. J. Mercer et al., Annarbor Sience, Ann Arbor, Michigan, 1983.

Yeh, T.-C., L. W. Gelhar and A. L. Gutjahr, Stochastic analysis of unsaturated flow in heterogeneous soils, 1, Statistically isotropic media, Water Resour. Res., 21(4), 447-456, 1985a.

Yeh, T.-C., L. W. Gelhar and A. L. Gutjahr, Stochastic analysis of unsaturated flow in heterogeneous soils, 2, Statistically anisotropic media with variable α, Water Resour. Res., 21(4), 457-464, 1985b.

Yeh, T.-C., L. W. Gelhar and A. L. Gutjahr, Stochastic analysis of unsaturated flow in heterogeneous soils, 3, Observations and applications, Water Resour. Res., 21(4), 465-471, 1985c.